Geophysical Constraints on Mantle Viscosity and its Influence on Antarctic Glacial Isostatic Adjustment

by

Andrea Darlington
B.Sc., University of Western Ontario, 2008

A Thesis Submitted in Partial Fulfillment
of the Requirements for the Degree of

MASTER OF SCIENCE

in the School of Earth and Ocean Sciences

Supervisory Committee

Geophysical Constraints on Mantle Viscosity and its Influence on Antarctic Glacial Isostatic Adjustment

by

Andrea Darlington
B.Sc., University of Western Ontario, 2008

Supervisory Committee

Dr. Thomas S. James (School of Earth and Ocean Sciences, Geological Survey of Canada)
Co-Supervisor

Dr. George D. Spence (School of Earth and Ocean Sciences)
Co-Supervisor

Dr. Stephane Mazzotti (School of Earth and Ocean Sciences, Université Montpellier)
Departmental Member

Abstract

Supervisory Committee
Dr. Thomas S. James (School of Earth and Ocean Sciences, Geological Survey of Canada)
Co-Supervisor
Dr. George D. Spence (School of Earth and Ocean Sciences)
Co-Supervisor
Dr. Stephane Mazzotti (School of Earth and Ocean Sciences, Université Montpellier)
Departmental Member

Glacial isostatic adjustment (GIA) is the process by which the solid Earth responds to past and present-day changes in glaciers, ice caps, and ice sheets. This thesis focuses on vertical crustal motion of the Earth caused by GIA, which is influenced by several factors including lithosphere thickness, mantle viscosity profile, and changes to the thickness and extent of surface ice. The viscosity of the mantle beneath Antarctica is a poorly constrained quantity due to the rarity of relative sea-level and heat flow observations. Other methods for obtaining a better-constrained mantle viscosity model must be investigated to obtain more accurate GIA model predictions.

The first section of this study uses seismic wave tomography to determine mantle viscosity. By calculating the deviation of the P- and S-wave velocities relative to a reference Earth model (PREM), the viscosity can be determined. For Antarctica mantle viscosities obtained from S20A (Ekstrom and Dziewonski, 1998) seismic tomography in the asthenosphere range from 10^{16} Pa·s to 10^{23} Pa·s, with smaller viscosities beneath West Antarctica and higher viscosities beneath East Antarctica. This agrees with viscosity expectations based on findings from the Basin and Range area of North America, which is an analogue to the West Antarctic Rift System.

Section two compares bedrock elevations in Antarctica to crustal thicknesses, to infer mantle temperatures and draw conclusions about mantle viscosity. Data from CRUST 2.0 (Bassin et al., 2000), BEDMAP (Lythe and Vaughan, 2001) and specific studies of crustal thickness in Antarctica were examined. It was found that the regions of Antarctica that are expected to have low viscosities agree with the hot mantle trend found by Hyndman (2010) while the regions expected to have high viscosity are in better agreement with the trend for cold mantle.

Bevis et al. (2009) described new GPS observations of crustal uplift in Antarctica and compared the results to GIA model predictions, including IJ05 (Ivins and James, 2005). Here, we have generated IJ05 predictions for a three layered mantle (viscosities ranging over more than four orders of magnitude) and compared them to the GPS observations using a χ^2 measure of goodness-of-fit. The IJ05 predictions that agree best with the Bevis et al. observations have a χ^2 of 16, less than the null hypothesis value of 42. These large values for the best-fit model indicate the need for model revisions and/or that uncertainties are too optimistic. Equally important, the mantle viscosities of the best-fit models are much higher than expected for West Antarctica. The smallest χ^2 values are found for an asthenosphere viscosity of 10^{21} Pa·s, transition zone viscosity of 10^{23} Pa·s and lower mantle viscosity of 2×10^{23} Pa·s, whereas the expected viscosity of the asthenosphere beneath West Antarctica is probably less than 10^{20} Pa·s. This suggests that revisions to the IJ05 ice sheet history are required. Simulated annealing was performed on the ice sheet history and it was found that changes to the recent ice load history have the strongest effect on GIA predictions.

Table of Contents

List of Tables

List of Figures

Acknowledgments

I would like to thank my supervisor, Tom James, for his support and guidance throughout the process of completing this research and for taking the time to teach an Astrophysics student the intricacies of the Earth science world.

Thanks also to my co supervisor George Spence and committee member Stephane Mazzotti whose insight and ideas were invaluable.

Thank you to Muriel Llubes, Nikolai Shapiro and Stefania Danesi for generously allowing me access to their data for this project.

I'd like to acknowledge all the staff at the PGC especially Roy Hyndman, whose research in North America became an entire chapter of this thesis, Robert Kung, whose assistance with ArcGIS was invaluable and Steve Taylor and Michelle Gorosh for their support with everything technical. Thanks as well to my fellow students at PGC including my office mates Natalie Balfour and Sabine Hippchen as well as Karen Simon for their advice and assistance.

Thanks to everyone in the School of Earth and Ocean Science at the University of Victoria especially Allison Rose for her guidance on administrative matters and Belaid Moa for his insight into programming on WestGrid.

An additional thanks to the Physics department at UVic for employing me as a teaching assistant during my time here and to the first year Physics lab staff led by Alex Wong. It's been an enjoyable learning experience.

Special thanks to friends from across the country including Janice Baker, Clio Bonnett, Miranda Brintnell, Erin Fedotov, Samantha Flood, Robbie Halonen, Stephanie Keating, Stephanie Langemeyer, Megan Mattos, Hazel McNeil and Albert Santoni for

their counsel and encouragement. Thanks to Colin and Gill Chadwick for making me feel at home in my home away from home. Thanks as well to Mike Dominy and the Westshore Community Concert Band, Nick LaRiviere and JIVE and Joe Hatherhill and Saxamaphone for filling my spare time with great music.

Finally, thanks to my family, Cara, and Jonas for their continued support and companionship.

Dedication

To my parents, for giving me the freedom to try just about anything and for being there when it went wrong.

Chapter 1 – Introduction

1.1 Overview

Covered almost entirely by ice and isolated at the South Pole, Antarctica is one of the least understood regions of the world. Changes to the ice sheets in Antarctica can, however, contribute to world wide effects on sea level and climate. The continent can be divided into two different regions: East Antarctica, which is cratonic in nature with a thick lithosphere and high bedrock elevations, and West Antarctica, which has a thin lithosphere and is home to a failed continental rift system (the West Antarctic Rift System or WARS) (van Wijk et al., 2008). Both areas are covered by large ice sheets and fluctuations in the size of these ice sheets drive bedrock motion.

The location and physical characteristics of Antarctica make obtaining data difficult and thus assumptions must be made on relatively little information. Models of processes such as glacial isostatic adjustment (GIA) must assume a viscosity for the mantle in order to obtain vertical crustal motion predictions (Ivins and James, 2005). Unlike the northern hemisphere, there are relatively little data (especially paleo-sea-level data) that can be used to infer a value for the mantle viscosity. The goal of this study is to determine a plausible viscosity profile for the mantle beneath West Antarctica. This is achieved by examining seismic S-wave velocity variations in the mantle and equating them to variations in the temperature and thus viscosity. Comparisons between GIA and GPS observations and vertical crustal motion model predictions are then performed to determine which of the wide range of viscosity profiles best fits the observations of uplift. Regions similar to West Antarctica exist in more heavily studied regions such as the Basin and Range in the United States and the East African Rift System. Viscosity

values from these regions thus give us an idea of plausible viscosity values for West Antarctica. If best-fit viscosity profiles agree with these estimated viscosities that would indicate that IJ05 is properly simulating GIA, whereas viscosity profiles with poorer fits (as are seen in this study) may indicate that revision to IJ05 is necessary.

This chapter commences by discussing the tectonic setting of Antarctica and the past ice thicknesses that have existed in the Antarctic ice sheets. An introduction to glacial history, as well as the methods used to infer it, follows.

1.2 Tectonic Setting

Although seismicity is low in Antarctica, there are still tectonic forces at work. The division between East and West Antarctica is marked by the presence of the Transantarctic Mountains (TAM) which lie on the border of the West Antarctic Rift System (WARS) (Figure 1.1). The Transantarctic Mountains (TAM) extend 3500 km across the entirety of Antarctica from Cape Adare in Victoria Land to Coats Land and are between 100 km and 300 km wide. The WARS experienced extension over a wide area in the past and may still experience some extension in more restricted regions today. Additionally, regions of active tectonics, including subduction and mid-ocean ridge spreading, exist near the tip of the Antarctic Peninsula (Maldonado et al., 1994).

1.2.1 West Antarctic Rift System

1.2.1.1 Continental Rifting

Continental rifts are areas where the lithosphere is deformed extensionally. In general these rifts are characterized by rift valleys flanked by normal faults with dips less than 60^{o}, large gravity lows, thin lithosphere and crust, volcanism, high heat flow, and

Figure 1.1: The regions of Antarctica (WARS – West Antarctic Rift System).

shallow seismicity caused by tensional stresses. They usually occur in areas with pre-existing weaknesses (Kearey et al., 2009).

Rifting can occur in two ways; actively and passively. In active rifting upwelling magma forces a rift to open. Doming occurs first, followed by the actual rifting. In passive rifting, the stretching and rifting occur first, followed by crustal subsidence.

There are two main kinds of continental rifts: Narrow rifts form where the lithosphere is cool, strong and thick, whereas wide rifts form where the lithosphere is hot, weak and thin. Narrow rifts are characterized by asymmetric rift basins, shallow seismicity, local crustal thinning, a high heat flow and a low velocity, low density mantle.

Wide rifts have broadly distributed deformation, heterogeneous crustal thinning, a thin mantle lithosphere, a high heat flow and normal faulting of various magnitudes. It's possible that the WARS may have experienced both of these rifting types. Over its history, the WARS started out as a wide rift (between 105 Myr and 65 Myr ago) but became narrower as the crustal weakness began to focus rifting into smaller regions (after 65 Myr ago) (Kearey and Vine, 1996).

Continental rifting can be associated with the break-up of continents when oceanic lithosphere forms in the area of thinned crust. Failed rift systems occur when the spreading slows down considerably or stops entirely, thus stopping the process of rifting before the continents fully separate. The West Antarctic Rift System is considered a failed rift system. Wide rifting became focused to a small area in the Victoria Land Basin (Figure 1.1), and movement eventually ceased on most of the rest of the rift (Huerta and Harry, 2007). Studies suggest that West Antarctica is currently moving at a velocity of less than 2 mm/yr away from East Antarctica in the direction of the South Georgia Islands (Dietrich et al., 2004, van Wijk et al., 2008). The West Antarctic Rift System is believed to be the source of recent volcanic activity in Antarctica and may even have an influence on ice flows in West Antarctica (Behrendt et al., 1996).

1.2.1.2 Topography

The WARS exists adjacent to the East Antarctic craton and within the younger, thinner lithosphere of West Antarctica. The WARS is made up of a number of shorter rifts crossing the continent. Along the southern portion of the rift is the Victoria Land Basin, where most recent crustal extension is thought to have occurred, as well as the Transantarctic Mountains. The mountains (on one side of the asymmetrical rift) are made

up of a 3000 km long rift shoulder escarpment of about 5 km in height. On the northern boundary of the rift system there is a region of intraplate volcanism called the Marie Byrd Land (MBL) dome. The MBL dome may be generated by a hotspot (Winberry and Anandakrishnan, 2004).

1.2.1.3 Tectonic Evolution

In the late Cretaceous extension began in most of West Antarctica (Huerta and Harry, 2007). This lasted until the late Palaeogene when the extension became more confined to the Victoria Land Basin. The transition between the two phases seemingly occurred at the same time as volcanic activity and strike-slip faulting in the Transantarctic Mountains. The early stage of extension was distributed throughout the weak accreted lithosphere in West Antarctica but after some time the deformation began to concentrate around a secondary weakness near the Victoria Land Basin. The change between diffuse and concentrated extension occurred when the thinned lithosphere allowed the upper mantle to decrease in temperature. This resulted in strengthening of the lithosphere, concentrating the extension in the weakest region, directly adjacent to the East Antarctic craton. The thicker lithosphere there allowed for a warmer upper mantle. This eventually resulted in the formation of the Terror Rift in the Victoria Land Basin.

1.2.1.4 Analogous Locations

The WARS is not the only rift system of its kind on the Earth. Two regions in particular have experienced similar extension of continental crust: the East Africa Rift and the Basin and Range region of North America (Kearey et al., 2009).

Like ice, water also weighs down the lithosphere on which it sits. Lake Bonneville (the largest of the late Pleistocene lakes in the Great Basin of the western

United States) once covered 49 000 km^2 and had a maximum depth of 340 m, thus causing a deformation in the lithosphere. Since then the lake has shrunk significantly, leaving several past shorelines visible. As water dissipates from the lake, the lithosphere rebounds to account for the decrease in the surface load.

Two prominent shorelines have been identified, mapped, and dated that are related to past stages of Lake Bonneville. Since the shorelines would have formed on a level surface, the present-day deformation indicates the amount of relative vertical deformation since the shorelines were formed. Modelling of the shoreline deflection caused by the changing water load allows determination of mantle viscosity. Using the Provo (most visible past shoreline) and Bonneville (extent of the lake when it was at its largest) shorelines and time between the two events (determined from radio carbon dating organic samples collected from the shorelines) the effective viscosity was determined. It was found to be much lower than many regions of the world. Minimum viscosity values of 4×10^{17} Pa·s were found at 40 km depth (Bills et al., 1994). Between 150 km and 300 km depth the viscosity rises to 2×10^{20} Pa·s. The nearby Lake Lahontan predicts viscosities with a minimum value of 5×10^{17} Pa·s (Bills et al., 2007).

In the East African Rift system the Rwenzori Mountains are among the highest mountains in Africa. Wallner and Schmeling (2010) suggest that the mountains were formed during rifting when the low viscosity and strength in the lowermost crust (created by the propagating rift tips surrounded by older lithosphere) resulted in delamination of the mantle lithosphere root. The unloading resulted in the rapid uplift of the less dense Rwenzori block, thus creating the mountains. Testing this theory numerically, they find

that the viscosity of the mantle beneath the East African rift ranges from 10^{25} Pa·s in the lithosphere to about 10^{19} Pa·s at a depth of 400 km.

Due to the similarities between these regions and the WARS area (Table 1.1), it is expected that mantle viscosities beneath West Antarctica should be similar to the values found in these studies.

1.2.2 Antarctic Peninsula

1.2.2.1 Subduction Zones

Subduction occurs when an oceanic tectonic plate slides beneath an oceanic or continental tectonic plate. The lower plate descends into the mantle and, frequently, the convergence of the two plates creates a compressional orogen. Seismicity is quite common on this type of plate boundary, both in the orogen, owing to continuing compression, and on the boundary between the two plates. The subducting plate can become locked for extended periods of time. When the "locked zone" on the plate boundary ruptures, a large earthquake is generated. Subduction zones can also create volcanic arcs on the upper plate.

Table 1.1: Comparison of the Basin and Range, East African Rift and West Antarctic Rift System.[1]

Rift	Lithosphere Thickness	Asthenosphere Viscosity	Width of Extension	Volcanism?	Narrow or Wide Rifting	Velocity of Rifting
Basin and Range	50-80 km [6]	10^{17} Pa·s - 10^{20} Pa·s [2]	120 km – 150 km [9]	Yes [10]	Wide [9]	11 mm/yr [1]
East African Rift	65 km [11]	10^{19} Pa·s - 10^{25} Pa·s [8]	40 km – 200 km [11]	Yes [11]	Narrow [11]	6 mm/yr [4]
West Antarctic Rift	80 km [5]	~10^{19} Pa·s - 10^{20} Pa·s	200 km – 300 km [5]	Yes [5]	Wide transitioning to narrow [5]	< 2 mm/yr[3,7]

[1] [1]Bennett et al. (2003), [2]Bills et al. (1994), [3]Dietrich et al. (2004), [4]Fernandes et al. (2004), [5]Huerta and Harry (2007), [6]Liu et al. (2011), [7]van Wijk et al. (2008), [8]Wallner and Schmeling (2010), [9]Wernicke (1992), [10]Zandt et al. (1995), [11]Zeyen et al. (1997)

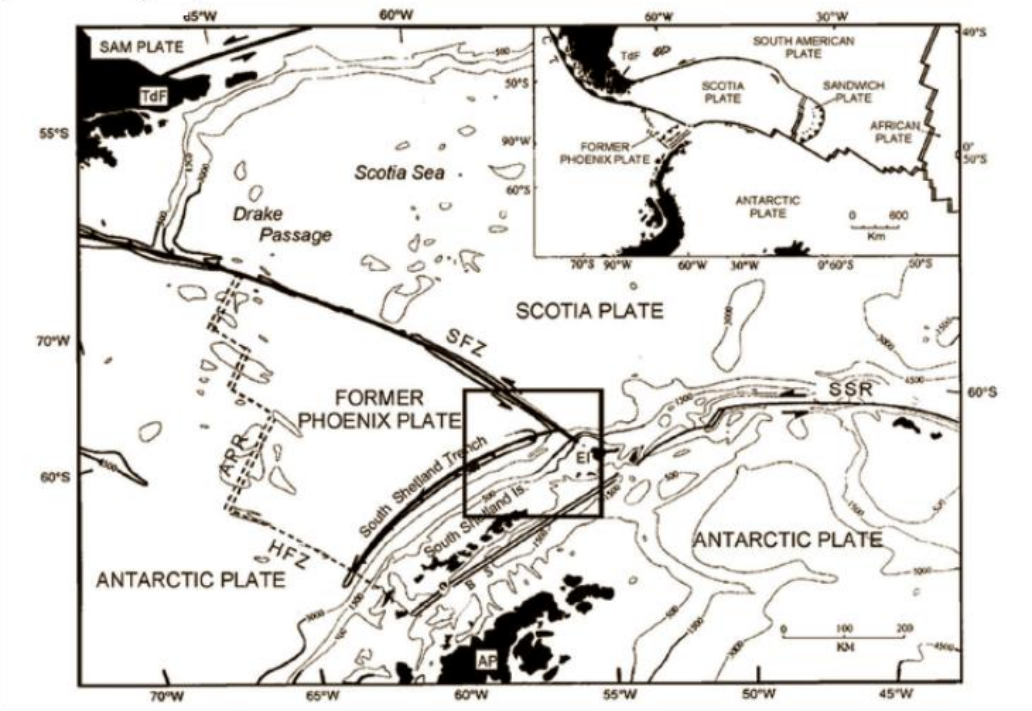

Figure 1.2: Plate boundaries surrounding the Antarctic Peninsula including the Scotia Plate, Antarctic Plate and Former Phoenix Plate (APR – Antarctic-Phoenix spreading ridge, BS – Bransfield Strait, EI – Elephant Island, HFZ – Hero Fracture Zone, SAM – South American, SFZ – Shackleton Fracture Zone, SSR – South Scotia Ridge, TdF – Tierra del Fuego) (Jin et al., 2009).

An intersection between two transform fault systems occurs near the northern tip of the Antarctic Peninsula (Klepeis and Lawver, 1996). The Shackleton Fracture Zone (SFZ) and the South Scotia Ridge (SSR) intersect with an angle of 70˚ between them. Immediately southwest of the intersection between the SSR and the SFZ lies the Shetland plate, a very small and young plate. Northwest of it lies the South Shetland Trench. Despite the fact that seafloor spreading is no longer occurring at the Drake Rise (located on the opposite edge of the Former Phoenix plate from the South Shetland Trench) slow subduction may still be ongoing at the trench due to slab-pull forces.

1.2.2.2 Tectonic Evolution

In the late Cenozoic the Phoenix plate to the west of the Antarctic Peninsula was subducting beneath the continental lithosphere of the Antarctic plate (Maldonado et al., 1994). Northwest of this, new oceanic crust was being created along the Antarctic-Phoenix ridge. At some point during the late Pliocene the ridge stopped producing crust and the rate of convergence at the subduction zone decreased significantly. By 5.5 Myr BP the Phoenix plate was almost entirely subducted (resulting in a collision between the ridge and the South Shetland trench) possibly causing uplift in the region of the Antarctic Peninsula and South Shetland Islands through the subduction of the Hero Fracture Zone on the south edge of the Phoenix plate. This period of uplift may have been followed by a period of subsidence in the region.

1.3 Glacial History

Antarctica hosts both the largest ice sheet in the world in the East Antarctic Ice Sheet (EAIS) and a large marine-based ice sheet with the West Antarctic Ice Sheet (WAIS). Owing to its size and location at the South Pole, Antarctica has a dominant influence on its own climate and on the surrounding ocean. Cold conditions are experienced even during the summer so surface melting of the ice sheets is not abundant, even near the coast. Instead, basal melting and iceberg calving are the main sources of ice loss for the ice sheets that cover the continent (Rignot and Thomas, 2002).

Ice-sheet histories vary with warmer and colder periods in the world's history and markers of these changes are required if we wish to study processes such as glacial isostatic adjustment (GIA). Long periods of time where lower than average temperatures are present are called glacial periods, while shorter periods of relative warmth are interglacial periods. Glacials can last for 40 kyr to 100 kyr while interglacials last for 10

kyr to 30 kyr. Typically, average temperatures can vary ~ 7 K between these two extremes (Lemke et al., 2007).

Ice sheet history since the time of the last glacial maximum (LGM) approximately 21 kyr ago has the largest effect on the present day GIA response. Ascertaining current and past ice thicknesses is done through glaciological, geological and geophysical investigations and analyses.

1.3.1 Present Day Mass Balance

The mass balance of a glacier or ice sheet is the amount of mass it is gaining or losing. It is derived from observations of the amount of precipitation entering an ice sheet and the amount of water leaving an ice sheet. There are three ways to measure the mass balance of an ice sheet:

a) The mass budget method, which compares mass gain through precipitation with mass loss through melting and calving (often with the use of ice cores). Accumulation is primarily obtained through snow pits, stakes and ice-core measurements. Combining a model of elevation (obtained through satellite radar altimetry) with in situ observations and knowledge of zero accumulation areas (regions where no significant precipitation accumulation is experienced) as well as the flow rates of outlet glaciers on the continent, Antarctica's ice flow basins can be delineated (Rignot and Thomas, 2002) (Figure 1.3). This indicates how much mass is being lost from the continent. The total net mass balance for the Antarctic ice sheet during the year 2000 was -138 ± 92 Gt/yr (Rignot et al., 2008).
b) Measurements of the change in ice elevation. These are translated into measurements of volume change, when combined with predictions of the vertical motion of

underlying ground associated with isostatic rebound or tectonics. Between 1992 and 2003, satellite radar altimetry shows that 72 % of the grounded ice sheet in Antarctica gained 27 ± 29 Gt/yr (Wingham et al., 2006).

c) Weighing of the ice sheets using satellite gravity measurements. The Gravity Recovery and Climate Experiment (GRACE) and the Ice, Cloud and Land Elevation Satellite (ICESat) launched by NASA are satellite missions that provide measurements of gravity change and elevation, respectively. After corrections for the GIA signal (provided by GIA models), these data can be used to determine the mass balance of the Antarctic Ice Sheet equivalent to a sea level change of 0.3 mm/yr (Wahr et al., 2000). Mass loss in Antarctica was measured to be 104 Gt/yr between 2002 and 2006 but it increased to 246 Gt/yr between 2006 and 2009 (Velicogna, 2009).

1.3.2 Methods for Determining Ice Sheet History

Ice-sheet history can be more difficult to determine. Samples must be collected from various sources and dated to give a measurement of when ice formed at or retreated from a given location. Dating techniques vary based on the type of sample collected.

1.3.2.1 Types of Samples

1.3.2.1.1 Lacustrine and Marine Sediments

Sediments are described as lacustrine when they were deposited in current or former lakes and marine when deposited in the ocean. Organic materials in these sediments can be dated using radiocarbon methods. Generally, in a formerly glaciated region, the earliest dated organic material gives a minimum age on the time of ice retreat from the area.

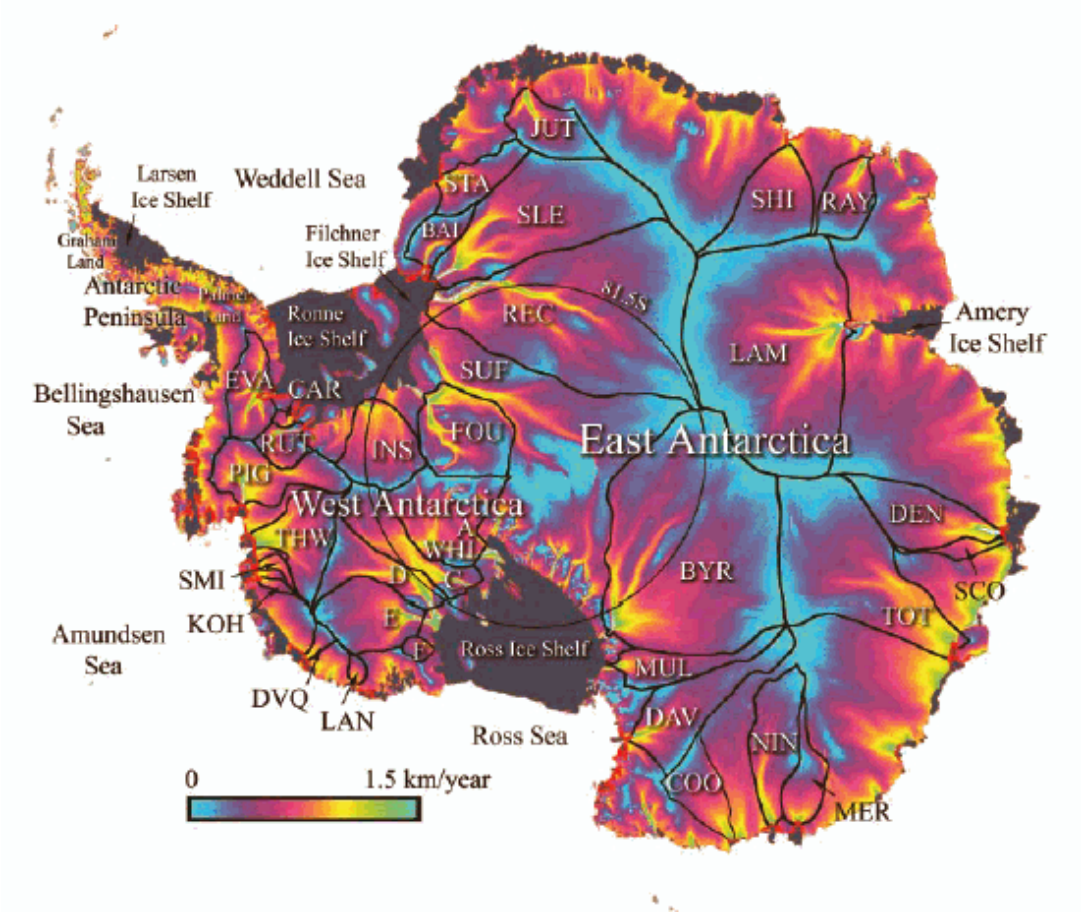

Figure 1.3: Calculated ice sheet balance velocity for 33 Antarctic glaciers. Catchment basin boundaries are black, grounding lines are red, and ice shelves are gray. Colour scale is linear. Glaciers: Pine Island (PIG), Thwaites (THW), Smith (SMI), Kohler (KOH), DeVicq (DVQ), Land (LAN), Whillans(WHI), A-F (A-F), Byrd (BYR), Mulock (MUL), David (DAV), feeding eastern Cook Ice Shelf (COO), Ninnis (NIN), Mertz (MER), Totten (TOT), Denman (DEN), Scott (SCO), Lambert/Mellor/Fisher (LAM), Rayner (RAY), Shirase (SHI), Jutulstraumen (JUT), Stancomb-Wills (STA), Bailey (BAI), Slessor (SLE), Recovery (REC), Support-Force (SUF), Foundation (FOU), Institute (INS), Rutford (RUT), Carlson (CAR), and Evans (EVA) (Rignot and Thomas, 2002).

1.3.2.1.2 Ice Cores

Many ice cores have been taken in Antarctica. These cores can be used to analyse the climate the continent was experiencing at a given time. Typically $\delta^{18}O$ concentration is measured at different depths in the sample. With an accumulation history and ice flow model accumulation rates of ice can be determined (Watanabe et al., 2003).

1.3.2.1.3 Moraines and Erosional Trimlines

Moraines are glacially formed accumulations of debris present in both currently and formerly glaciated regions. Erosional trimlines are points where the age or amount of erosion differs. These two features can be used to determine the maximum thickness of ice sheets as material left from the glacier and erosion it caused are still present and visible on the rocks.

1.3.2.1.4 Volcanic Nunatak

When volcanoes erupt in glaciated regions the tephra and lava flows are quickly buried by ice sheets. These rocks are ideal for exposure dating if they have not been in the ablation zone of a moraine long (Ackert et al., 1999).

1.3.2.2 Dating Techniques

1.3.2.2.1 Radiocarbon Dating

Radiocarbon dating involves measuring the amount of radioactive carbon (^{14}C) present in an organic sample. When a plant or animal dies it ceases to absorb further ^{14}C so, after making an assumption about the levels of ^{14}C in the atmosphere at the time of its death, the age *t* can be calculated according to

(1-1) $$N = N_0 e^{-\lambda t}$$

(1-2) $$\lambda = \frac{\ln 2}{t_{1/2}}$$

where N_0 is the number of atoms at t=0, N is the number of atoms present now, and lambda is the decay constant. The half-life $t_{1/2}$ of 14C is 5730 yr.

1.3.2.2.2 Thermoluminescence Dating

Thermoluminescence dating measures the accumulated radiation a material (with crystalline components) has absorbed since the material was cooled from a high temperature. Heating during the measurements creates a weak light signal that is proportional to the amount of radiation absorbed by the sample. The ionizing dose received from radioactive elements in the soil or from cosmic radiation is assumed to be proportional to age.

1.3.2.2.3 Surface Exposure Dating

Surface exposure dating encompasses all techniques that measure the length of time that a given rock has been exposed to the Earth's atmosphere. Most commonly the rocks are dated through cosmogenic nuclides.

Cosmic rays hitting exposed rock can dislodge protons or neutrons from a given atom. This creates either another type of atom or a different isotope, referred to as a cosmogenic nuclide. Measuring the concentration of these elements in a rock sample and making assumptions about the flux of cosmic rays, the length of time that the given rock has been exposed to cosmic rays can be calculated. ^{10}Be and ^{26}Al are the most commonly used elements because they result from the original elements ^{16}O and ^{28}Si; both are quite common in crustal material.

1.3.2.3 Modelling Methods

1.3.2.3.1 Climate and Ice-Flow Modelling

Accumulation of ice and snow is dependant on the rate of precipitation in a given area. Climate models can make predictions about the amount of snowfall seen in Antarctica and, thus, how much ice mass was being added to various regions.

Models of ice flow can combine several of the data gathering methods discussed above. Using the available data these models can help to obtain the ice-sheet histories in areas and times where data are unavailable or difficult to obtain.

Climate modelling methods can only be applied to the past few decades. Present rates of snow fall and melting cannot accurately be extrapolated into the distant past as is necessary in glacial isostatic adjustment modelling. Glaciological models must be used if we wish to use ice-sheet histories that are viable to the LGM.

1.3.3 Antarctic Observations

1.3.3.1 East Antarctica

East Antarctica has seen significantly less change in ice thickness since LGM than other regions of the continent. Toracinta et al. (2004) modelled climate world wide at Last Glacial Maximum and found that precipitation was very low in the southernmost regions of the world leading to little accumulation during that time. There are three major regions in Wilkes Land, East Antarctica that are currently ice-free and thus moraine and lacustrine deposits can be dated. At Vestfold Hills (Figure 1.4), south of the Lambert Glacier, Zwartz et al. (1998) studied sediment cores from lakes that were once connected with the ocean. Regional unloading was largely complete by 7 ^{14}C kyr BP. They suggest that the ice sheet in the area has thinned by 600 m to 700 m since LGM. The nearby Larsemann Hills however were unloaded by 13.5 kyr BP as indicated in dating (including radiocarbon dating, thermoluminescence dating, inorganic and microfossil analysis and

ecological modelling) of siliceous microfossils from sediment cores (Verleyen et al., 2004). The third location is the Bunger Hills and the Wind Mill Islands where optically stimulated luminescence dating of sediments on the shorelines of ancient lakes show that the southern hills were exposed by 20 kyr BP (shortly after LGM) and complete deglaciation occurred by 9.2 kyr BP (Gore et al., 2001). Relative sea level curves created through the use of radiocarbon dating of marine to freshwater transitions adjacent to the Lambert Glacier indicate that ice initially retreated between 15.4 kyr and 12.6 kyr BP. Glaciers likely readvanced during the mid Holocene before retreating again later in that time period (Verleyen et al., 2005). Mac. Robertson Land was investigated by Mackintosh et al. (2007) using single isotope analysis (^{10}Be and ^{26}Al) to determine mean boulder ages. The region likely thinned by less than 350 m in the last 13 kyr, most of this occurring between 12 kyr and 7 kyr BP. Ice thicknesses in East Antarctica seem to have been relatively constant both over time and space. Watanabe et al. (2003) compared several ice cores, specifically Dome Fuji and Vostok in East Antarctica and find that they are very similar with respect to their ^{18}O record. In the Shackleton Range on the border between West and East Antarctica, Fogwill et al. (2004) studied concentrations of the cosmogenic nuclides ^{10}Be and ^{26}Al on surface rock outcrops. Moraines found between 200 m and 340 m above the outlet glaciers are found and likely represent the maximum thickness of the Filcher-Ronne Ice Shelf. Recession from LGM had been underway for a significant period of time before the arrival of the Holocene. Many regions had ice thicknesses similar to those existing today indicating limited thickening on the high and interior regions of the ice sheet (Hall, 2009). A summary of this data is given in Table 1.2.

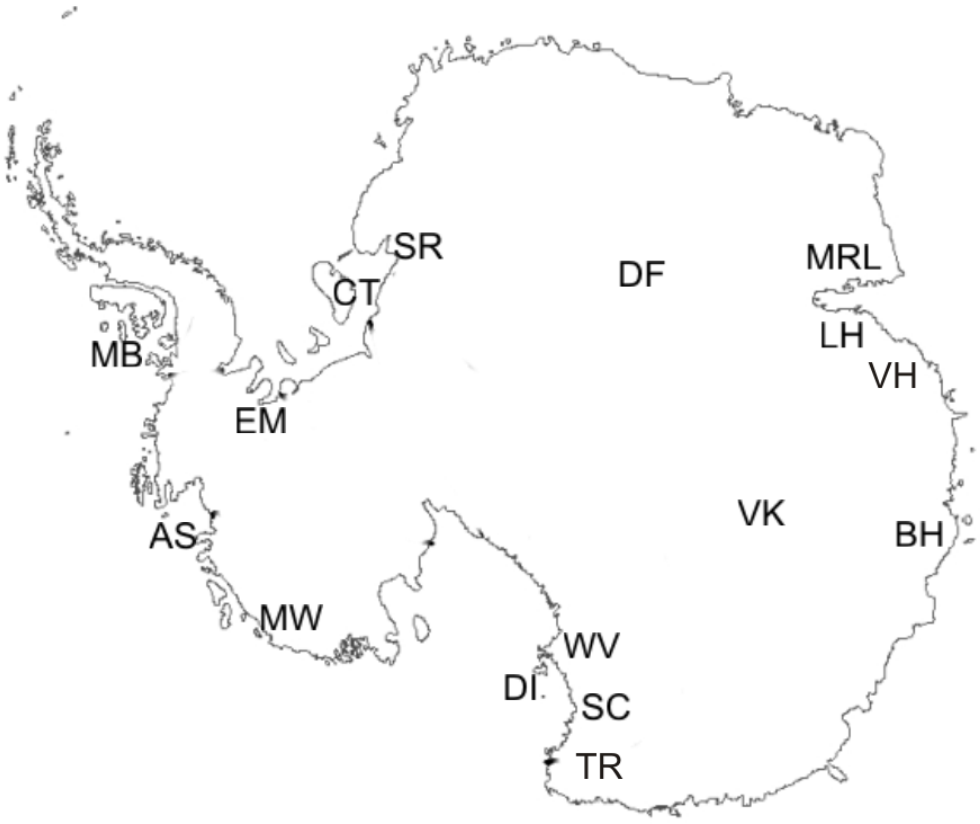

Figure 1.4: Locations where ice thickness data was obtained (AS – Amundsen Sea, BH – Bunger Hills, CT – Crary Trough, DF – Dome Fuji, DI - Dunlop Island,EM – Ellsworth Mountains, LH – Larsemann Hills, MB – Marguerite Bay, MRL – Mac Robertson Land, MW – Mount Waesche, SC – Scott Coast, SR – Shackleton Range, TR – Terror Rift, VH – Vestfold Hills, VK - Vostok, WV – Wright Valley).

1.3.3.2 Weddell Sea and Antarctic Peninsula

The Weddell Sea sector of the former expanded Antarctic ice sheet may have made a large contribution to the global water balance since the Last Glacial Maximum. It drains the East Antarctic Ice Sheet in the east, the West Antarctic Ice Sheet in the south and ice caps in the west, making it an ideal area for studying the history of these different glacial systems. Marine evidence including tills located near the current sea floor indicate that ice sheets were grounded in Crary Trough (located in the southern Weddell

Sea) and on the Antarctic Peninsula during LGM. In Ellsworth and Palmer land the ice saw a thickening of ~ 400 m but on the Ellsworth Mountains the thickening was as large as 1900 m. By analysing the gas content of bubbles in Antarctic ice cores it is possible to determine the ice elevation at the time the accumulated snow compressed into ice. In the interior of the West Antarctic Ice Sheet this data suggests that the ice did not thicken and may even have thinned during LGM (Bentley and Anderson, 1998).

On the Antarctic Peninsula at Marguerite Bay a relative sea level curve was created by Bentley (2009) from radiocarbon dating of penguin remains and shells. With some extrapolation they found that the minimum date of deglaciation was 9 ^{14}C kyr BP. A time of decreased wave activity was inferred between 3.5 and 2.4 ^{14}C kyr BP, possibly a sign of a decreased summer sea ice extent in the region. The precise location of the Amundsen Sea grounding line during LGM is unknown but using multi-beam swath bathymetry and sonar records in the Amundsen Sea, combined with radiocarbon dating, Anderson et al. (2002) found that the ice sheet had advanced to at least the middle of the continental shelf.

1.3.3.3 Marie Byrd Land

Marie Byrd Land lies to the south of the Antarctic Peninsula and east of the Ross Sea. Dating of the volcanic material from Mount Waesche (a volcanic nunatak in the region) using ^{3}He and ^{36}Cl can be used to find past ice elevations. Ackert et al. (1999) found that the ice reached its maximum thickness in Marie Byrd Land as ice in the Ross Sea was already beginning to deglaciate (~ 10 kyr BP). At that time the ice may have been 45 m thicker than it is currently.

1.3.3.4 Ross Sea

During LGM the West Antarctic Ice Sheet advanced into the Ross Sea Embayment and combined with expanded outlet glaciers of the East Antarctic Ice Sheet. The ice sheet became grounded and approached the continental shelf edge (Denton and Hughes, 2000).

Deglaciation of the Ross Sea had a significant effect on global sea level. At points in the past the ice sheet there was grounded but it has since thinned to a floating ice shelf. Data in other parts of the world (e.g. Barbados) indicate that a meltwater pulse occurred at 14.2 kyr BP causing significant sea level rise (between 13 m and 25 m). Licht (2004) investigated how much of this pulse might have been caused by melting in the Ross Sea. Using ^{14}C analysis of marine geologic data it was found that the Ross Sea always contained enough ice to cause at least 3 m to 6 m of eustatic sea level rise. The contribution to the meltwater pulse from the Ross Embayment was likely less than 1 m in total. In the central Ross Sea, typical methods for obtaining ice history are impossible due to the lack of exposed bedrock. Waddington et al. (2005) create an ice flow model varying the accumulation rate and ice sheet thickness. They then compared the model results to ice cores taken in the region. The histories indicate that ice has thinned only 200 m to 400 m since LGM. Surface exposure dating in the Pine Island Glacier of ^{10}Be and ^{26}Al was performed by Johnson et al. (2008). Over the past 4.7 kyr the thinning rate in the region was found to be 3.8 cm/yr compared to present day rates of 1.6 m/yr (observed between 1992 and 1996). The rapid thinning of today could not have been sustained all the way back to the Holocene which is confirmed by similar past rates of ice thinning seen in the Smith and Pope glaciers.

1.3.3.5 Transantarctic Mountains

Radiocarbon dating of penguin remains, sealskin, shells and seaweed from raised beaches on the Scott Coast (southern Victoria Land) is used to create a relative sea level curve of the region in Hall et al. (2004). They find that, in this region, the final unloading of grounded ice occurred at about 6.5 ^{14}C kyr BP. Since then the sea level on the Scott Coast has fallen 32 m. Some anomalously old dates were found for penguin guano on Dunlop Island suggesting that ice heights may have been higher (~ 500 m) during the Holocene. To the north, in the Wright Valley, evidence has been found for a former glacial lake, Glacial Lake Wright. Lake sediments were found on the valley floor to an elevation of ~ 400 m and radiocarbon dating of algae indicates that at Last Glacial Maximum the lake may have been 550 m deep (Hall et al., 2001). At the Reedy glacier (located at the southernmost tip of the Ross Sea) Bromley et al. (2010) use glacial geologic mapping and ^{10}Be surface exposure dating and find that during the LGM, ice thickening was asymmetric. Near the head of the glacier ice was 40 m thicker than today but at the base the glacier was thicker by ~ 500 m. On the other side of the TAM, in East Antarctica, the ice sheet has changed very little since LGM. In the past 21 kyr the ice thickness has not changed more than 75 m (Ivins and James, 2005). West Antarctic ice thickness data is summarized in Table 1.3.

Table 1.2: Summary of Dates and Ice Thicknesses for East Antarctica[2]

Region	21 kyr – 10 kyr	10 kyr – 5 kyr	5 kyr – present
Vestfold Hills (Wilkes Land)		8 kyr – Regional unloading complete[4]	
Larsemann Hills (Wilkes Land)	13.5kyr – Regional unloading complete[4]		
Bunger Hills (Wilkes Land)	20 kyr – Southern hills exposed[2]	9.2 kyr – Regional unloading complete[2]	
Lambert Glacier	15.4 kyr- 12.6 kyr – Initial ice retreat[5]	8kyr-3 kyr – Readvance of ice[5]	Late Holocene – Ice retreat[3]
Mac. Robertson Land	12 kyr-7 kyr – Ice thins by less than 350 m[3]		
Shackleton Range	11.7 kyr-Present – Relatively constant ice thickness[1]		

[2] [1]Fogwill et al., 2004, [2]Gore et al., 2001, [3]Mackintosh et al., 2007, [4]Verleyen et al., 2004, [5]Verleyen et al., 2006

Table 1.3: Summary of Dates and Ice Thicknesses for West Antarctica[3]

Region	21 kyr – 10 kyr	10 kyr – 5 kyr	5 kyr – present
Ross Sea	21 kyr – WAIS advanced into Ross Sea Embayment and combined with EAIS (became grounded)[5]	Holocene – Ice thinned 200 m - 400 m[9]	
Pine Island Glacier			4.7 kyr-Present – Ice thinning rate changed from 3.8 cm/yr to 1.6 m/yr[8]
Crary Trough (Weddell Sea)	21 kyr – Ice sheet grounded[2]		
Ellsworth and Paler Land	21 kyr – Ice thickened ~ 400m (1900m in Ellsworth Mountains)[2]		
Marguerite Bay (Antarctic Peninsula)	10.2 kyr – Minimum date of deglaciation[3]		3.7 kyr-2.4 kyr – Decreased summer ice extent and wave activity[3]
Mount Waesche (Marie Byrd Land)	10 kyr – Ice reached maximum thickness (~45 m thicker than the present thickness)[1]		
Scott Coast (Victoria Land)		7.5 kyr – Regional unloading complete[7]	Sea level has fallen by 32 m[7]
Glacial Lake Wright (Wright Valley)	21 kyr – Lake depth at 500 m[6]		
Reedy Glacier	21 kyr-Present – Ice thinned 40 m at head of glacier, thinned 500 m at base[4]		

[3] [1]Ackert et al., 1999, [2]Bentley and Anderson, 1998, [3]Bentley, 2009, [4]Bromley et al., 2010, [5]Denton and Hughes, 2000, [6]Hall et al., 2001 , [7]Hall et al., 2004, [8]Johnson et al., 2008, [9]Waddington et al., 2005

Chapter 2 – Earth Rheology

2.1 Overview

Rheology describes the way in which a material flows. Mantle rheology has an important effect on how the crust responds to stress and, thus, to the process of glacial isostatic adjustment (GIA). This chapter will provide an introduction to the nature of the Earth's rheology and its effect on GIA.

2.2 Elastic Materials

At low pressure and temperature (in the upper lithosphere for example) rocks often behave elastically. In this case the stress is linearly proportional to the strain. An elastically deforming body will experience instantaneous deformation when a load is applied and instantaneous (and total) recovery when it is removed. In a solid, this elastic behaviour results from the interatomic forces holding each atom in its proper lattice location. Forces that move the atoms closer together or pull them apart are resisted by this interatomic force (Turcotte and Schubert, 2002). Any material that behaves elastically will only do so below a certain threshold stress which depends on the material in question as well as the temperature and pressure. Above this limit the rock will experience brittle or ductile deformation (Ranalli, 1995).

Mechanically, an analog for an elastic material is a spring. A force against the spring instantaneously stretches or compresses it but, should the force be removed, the spring immediately returns to its original shape. The linear stress-strain relationship for an isotropic elastic material is as follows:

(2-1) $$\sigma_{ij} = \lambda \varepsilon_{kk} \delta_{ij} + 2\mu \varepsilon_{ij}$$

where σ_{ij} are the components of stress for any point within the elastic material, δ_{ij} is the Kronecker delta, λ is Lame's first parameter, μ is the shear modulus, ε_{kk} is the change in volume per unit volume, or cubical dilatation, and ε_{ij} are the components of strain for any point within the elastic material.

2.3 Viscous Materials

Fluids experience steady-state flow under a constant stress. Instead of depending linearly on the strain as solids do, stress in a fluid is proportional to the strain rate. Newtonian fluids are those in which the stress-strain rate relationship is linear while non-Newtonian fluids experience a non-linear relationship between stress and strain rate. A dashpot represents a mechanical equivalent to this behaviour. It consists of a damper which resists movement by viscous friction. A force is created which opposes the velocity which slows the motion of the fluid. The relationship for Newtonian fluids is expressed in equation 2-2.

(2-2) $$\sigma_{ij} = -p\delta_{ij} + 2\eta \dot{\varepsilon}_{ij}$$

where p is the thermodynamic pressure, η is the Newtonian viscosity and $\dot{\varepsilon}_{ij}$ is the strain rate (Ranalli, 1995).

2.4 Viscoelasticity

A material that experiences both elastic and viscous deformation is referred to as viscoelastic. For instance, the mantle is a crystalline solid (thus it should behave elastically) but it also behaves as a viscous fluid over geologic time scales. The mantle deforms elastically on short time scales but viscously on long time scales thus making it a viscoelastic material.

2.4.1 Linear Rheology

Using a linear rheological model, elastic and viscous components can be combined in series (creating a Maxwell body) or in parallel (Kelvin body). Earth models typically use the Maxwell model which gives:

(2-3) $$\dot{\varepsilon} = \frac{\dot{\sigma}}{2\mu_M} + \frac{\sigma}{2\eta_M}$$

where μ_M is the rigidity and η_M is the viscosity. The i and j indices have been removed from the stress, strain and their derivatives for clarity. The Maxwell relaxation time of the mantle (using a viscosity of 10^{20} Pa·s and a rigidity of 6×10^{10} Pa) is approximately 50 years which is comparable with the characteristic time of glacial isostatic adjustment. Variations in viscosity result in large variations in relaxation time.

Combining the Kelvin and Maxwell methods to get a general type of linear rheology gives:

(2-4) $$2\eta_K \ddot{\varepsilon} + 2\mu_K \dot{\varepsilon} = \frac{\eta_K}{\mu_M}\ddot{\sigma} + (\frac{\eta_K}{\eta_M} + \frac{\mu_K}{\mu_M} + 1)\dot{\sigma} + \frac{\mu_K}{\eta_M}\sigma$$

where μ_K and μ_M are the rigidities for the Kelvin and Maxwell elements respectively and η_K and η_M are the viscosities of the Kelvin and Maxwell elements.

2.4.2 Non-Linear Rheology

Some viscoelastic materials do not experience a linear stress-strain rate relationship meaning that the above equations will not apply. These materials can move via two different methods of creep: diffusion and dislocation.

At low stress levels diffusion is the predominant method of creep. Atoms diffuse through the interiors of crystal grains when they are subjected to stress (Turcotte and Schubert, 2002). The relationship between stress and strain rate can be described as:

(2-5) $$\dot{\varepsilon} = A\frac{\sigma^n}{d^m}\exp(-\frac{Q+PV}{RT})$$

where Q and V are the activation energy and volume respectively, P is the pressure, R is the gas constant, T is the temperature, n is the power law exponent, d is the grain size and m is the dependence on the grain size and A is a material parameter. For diffusion creep n is typically 1 and m ranges between 2 and 3 depending on the type of creep. In the mantle olivine has an n value of 3.5 while spinel has a value of 2.0. For m, Nabarro-Herring creep has value of 2 while Coble creep has a value of 3 (Ranalli, 1995).

Stress can also cause the migration of dislocations (imperfections) within a crystalline solid. Dislocation creep occurs more often in high stress areas and thus is more applicable to the stress-strain rate relationship for the mantle. The relationship is shown below:

(2-6) $$\dot{\varepsilon} = A\sigma^n \exp(-\frac{Q+PV}{RT})$$

2.5 Viscosity

Viscosity is a measure of the resistance to motion of a fluid. In comparison to most everyday fluids, the Earth's mantle is highly viscous with viscosities ranging between 10^{19} Pa·s and 10^{24} Pa·s depending on depth, temperature, state of stress and composition of the mantle, among other things. The effective viscosity relates the stress to the strain rate according to:

(2-7) $$\sigma = 2\eta_{eff}\dot{\varepsilon}$$

In the case of diffusion creep, combining Equation 2-5 and 2-7 and using n=1 and m=3, the viscosity is:

(2-8) $$\eta_{eff} = \frac{RTh^3}{24V\delta D_{b0}} \exp(\frac{Q+PV}{RT})$$

where h is the length of one side of the original cube in the crystal and δD_{b0} is the change in frequency factor for the diffusion coefficient (Turcotte and Schubert, 2002).

For dislocation creep, the type of creep seen in the Earth's mantle, the equation becomes:

(2-9) $$\eta_{eff} = \frac{1}{2} \varepsilon^{*(1-n)/n} A^{-1/n} \exp(\frac{Q+PV}{nRT})$$

2.6 Inferences of Mantle Viscosity

There are several measurable quantities that can be used to infer the viscosity of the mantle, typically through obtaining a measurement of mantle temperature.

2.6.1 Temperature and Heat Flow

Heat flow measurements can be indicators of where temperatures rise rapidly with depth. Heat flow is defined as:

(2-10) $$q = -k \frac{dT}{dy}$$

where k is the coefficient of thermal conductivity, T is the temperature and y is the depth (positive downwards) (Turcotte and Schubert, 2002).

Most surface heat flow observations have been taken in the Northern Hemisphere and several regions, particularly ice covered regions such as Antarctica, have little to no heat flow data available at all. Since viscosity has been shown to be dependent on temperature many other methods for inferring viscosity focus on determining mantle temperature.

2.6.2 Seismic Wave Tomography

Seismic wave tomographic results are available globally, albeit with differing resolutions for different regions of the world. The velocities of seismic waves caused by earthquakes can be measured from stations around the world giving an approximation of mantle structure. In general fast velocities correspond to colder regions while slow velocities correspond to warmer ones. From this a temperature profile can be determined.

Shapiro and Ritzwoller (2004) use shear wave velocities to determine heat flow in regions where heat flow observations are not possible, such as Antarctica. They create a model that effectively matches the observed heat flow values found in areas where data are available and are similar in properties to East and West Antarctica. From this they can use the model to infer the heat flow values expected in Antarctica.

2.6.3 Sea Level Observations

Glacial isostatic adjustment (GIA) is the response of the Earth to changes in ice mass. It is still continuing at present because the interior of the Earth behaves viscoelastically. In regions that were formerly glaciated, the land was depressed. Now that the ice is gone, the land is rising (rebounding) to its former position of equilibrium which results in relative sea level change.

One method of measuring past sea levels is through old shorelines, regions where the remains of oceanic life is found above the current sea level or where remains of continental life are found below current sea levels. The fossils can be dated, giving an approximate age of the ancient shoreline. If the shoreline elevations and ages are known, then quantitative models of the GIA process can be developed and inferences of mantle viscosity made.

2.6.4 Volcanism and Xenoliths

Mantle xenoliths are mantle materials that were delivered to the surface through a volcanic eruption. Analysis of mantle xenoliths uses thermoluminescence dating to determine the temperature at which the xenolith crystallized. A xenolith's temperature of crystallization gives insight into the temperature of the mantle region in which it was formed, likely the upper mantle beneath the volcanic area it emerged from.

2.6.5 Elastic Lithosphere

At shallow depths in the Earth, the lithosphere deforms elastically for small deformations and through brittle faulting and earthquakes for larger ones. At greater depths, temperatures are too high for brittle behaviour so deformation is ductile, causing a reduction in strength. The Earth's crust is composed of silicate rocks such as basalt and granite which are less dense than rocks found in the mantle, which mainly has an olivine-based minerology. This difference in chemical compositions between the two layers leads to differences in mechanical behaviour.

In regions with high heat flow, the brittle-ductile transition is reached in the crust and this can define the thickness of the elastic lithosphere (Te) in some simple cases. In regions with very low heat flow this boundary is reached in the mantle. In intermediate temperature regions the definition becomes more complex as the combined effect of two or more elastic layers is required. In this case the effective elastic lithosphere thickness is an estimate of the thickness of an elastic layer with the same elastic bending properties that the lithosphere has. Flexure studies reveal that Te is the depth integral of the bending stress (Watts and Burov, 2003).

To estimate Te on the basis of rheology profiles, the elastic and ductile strength profiles are calculated. The brittle stress can be calculated from the formula below.

(2-11) $$\sigma = \alpha \rho g z (1 - \lambda)$$

where α is a numerical parameter that depends on the faulting, ρ is the average density, g is the gravitational acceleration, z is the depth and λ is the pore fluid factor.

Ductile deformation occurs through dislocation creep as described. The ductile stress can be calculated by rearranging Equation 2-6 as follows:

(2-12) $$\sigma = \left(\frac{\dot{\varepsilon}}{A}\right)^{1/n} \exp\left(\frac{Q + PV}{nRT}\right)$$

The 'strength' is defined as the lower of the brittle and ductile stress differences at a given depth (Ranalli, 1995).

The thickness of the elastic lithosphere controls how the lithosphere deforms when it is loaded. Lithosphere thicknesses can vary from thin (<20 km) to very thick (~200 km).

2.7 Inferences of Effective Elastic Lithosphere Thickness

2.7.1 Flexural Rigidity

The way the Earth deforms to a load gives important information about thermal, physical and mechanical properties of the lithosphere. Through flexural isostasy the lithosphere remains in gravitational equilibrium. The deflection of a plate depends on its rheology and mechanical properties. The flexural rigidity is defined as

(2-13) $$D = \frac{E T_e^3}{12(1 - \upsilon^2)}$$

where T_e is the elastic lithosphere thickness, E is Young's modulus and ν is Poisson's ratio (Turcotte and Schubert, 2002).

Flexural rigidity can be used to determine the elastic lithosphere thickness through two different methods. The first is the admittance method (Lewis and Dorman,

1970) using free air gravity anomalies. The free air gravity anomaly depends on the measured gravity, the elevation and a reference geoid.

The second method is through the coherence method (Forsyth, 1985) using Bouguer gravity data. The Bouguer gravity anomaly depends on the free air gravity anomaly and the crustal density.

For large flexural wavelengths a topographic load on the surface will bend the lithosphere resulting in a negative Bouguer anomaly. At these wavelengths the topography and Bouguer gravity anomaly correspond closely. At short wavelengths the topography is largely supported by stresses in the elastic lithosphere. The thicker or stiffer the elastic plate is, the longer the wavelength of transition required. Therefore the plate thickness that best fits the coherence can be used as a measure of the thickness of the elastic lithosphere (Turcotte and Schubert, 2002).

2.8 Glacial Isostatic Adjustment (GIA)

In comparison to other geologic processes, the growth and melting of ice sheets occurs relatively quickly. When ice forms on the surface of the Earth its weight pushes down on the crust resulting in lateral movement of the mantle material below and depression in the crust. The short time scale over which this occurs means that the dynamic effects caused are important in the adjustment of the mantle to the changing surface load. When the ice melts the weight is lessened and the crust begins to rebound as the mantle material returns. The surface displacement for a uniform half space at a specified time following assumed instantaneous unloading is given by

$$w = w_m \exp(\frac{-t}{\tau_r}) \tag{2-14}$$

where w_m is the original displacement, t is time and τ_r is the relaxation time given below:

(2-15) $$\tau_r = \frac{4\pi\eta}{\rho g \lambda}$$

where η is the viscosity, ρ is the density, g is the force due to gravity and λ is the wavelength of the load (Turcotte and Schubert, 2002).

The speed and amount of rebound that occurs is dependant on the ice sheet history in the region and the Earth rheology beneath it. Mantle viscosity, ice thickness, composition and effective elastic lithosphere thickness all have an effect on vertical crustal motion rates.

2.8.1 Measuring Glacial Isostatic Adjustment

2.8.1.1 Sea Level Observations

As rebound of the crust occurs the relative sea level on the coast will decrease. Dating markers of past sea levels can give measurements of sea level height at different times and thus the amount the landmass has risen between that time and the present. Sea level curves for Antarctica are nearly nonexistent as obtaining dating markers is very difficult.

2.8.1.2 Global Positioning System

GPS stations set up at the same point annually over several years can give a measure of vertical crustal motion. Each year the measurement of the position in an area that is rising or falling will be slightly different. With data from several years available, the rate at which the crust is rebounding can be calculated and then compared to the predictions of GIA models.

Chapter 3 – Using Seismic Wave Tomography to Determine Mantle Viscosity

3.1 Overview

Events that impart low frequency elastic energy into the Earth, such as earthquakes or explosions, create waves that travel all over the world. These seismic waves travel at different speeds depending on the temperature and composition of the materials they are travelling through. Measuring the time between an event and the arrival of seismic waves at a given point (for several events) can give valuable information about the nature of the mantle.

3.2 Seismic Tomography

Imaging of the Earth's mantle and other layers is done using seismic tomography. Travel times (the time between the event that produced the seismic waves and the time the waves were observed at a given station) are recorded for seismic waves and the velocity is calculated. The velocity changes with temperature and composition of the rocks it is travelling through and thus, after numerous travel-times have been observed, seismic velocity profiles can be developed for the Earth. The seismic velocities depend on density and elastic parameters of the Earth, which are different for different minerals and hence for different rocks, and on temperature. Spatial variations (especially lateral variations) in the seismic velocities within the mantle have been linked to temperature differences (Ranalli, 1995). Seismic waves come in several forms all of which travel differently through a medium.

3.2.1 Types of Seismic Waves

3.2.1.1 P-waves

P-waves or compressional waves are the highest velocity seismic waves. The particles in the material vibrate in the direction of propagation (they are longitudinal waves) and thus are made up of compressions and rarefactions. P-waves can travel through solid, liquid or gaseous materials.

In a homogeneous, isotropic medium the velocity of a P-wave can be expressed as:

(3-1) $$v_p = \sqrt{\frac{\lambda + 2\mu}{\rho}} = \sqrt{\frac{k + 4/3\,\mu}{\rho}}$$

where λ is the first Lamé parameter, μ is the shear modulus, ρ is the density and k is the bulk modulus of the substance the wave is travelling through (Ranalli, 1995).

3.2.1.2 S-waves

S-waves or shear waves arrive following P-waves. In shear waves the particles on the wavefront vibrate in a direction perpendicular to the direction of propagation. Unlike P-waves, S-waves cannot travel through liquids or gases meaning that they can not propagate through the liquid outer core of the Earth.

In a homogeneous, isotropic medium S-wave velocity can be expressed as:

(3-2) $$v_s = \sqrt{\frac{\mu}{\rho}}$$

3.2.1.3 Surface Waves

Instead of travelling through the Earth, surface waves travel along the surface. Surface waves encountered in seismology have two mechanical types; Love waves and

Rayleigh waves. Love waves experience transverse motion (similar to S-waves) while Rayleigh waves experience both transverse and longitudinal motion.

3.2.2 Antarctic Tomography

Seismic records are rare in Antarctica due to the remote nature and difficult logistics of the continent. As well, Antarctica has a relatively low level of seismicity, meaning that local seismic wave sources are relatively sparse. Consequently, local tomographic velocity models of the region are rare. For this study, results of global tomographic inversions are employed. Ekstrom and Dziewonski (1998) created a world wide model of seismic S-wave velocities in the mantle. This seismic tomographic model was obtained using absolute and differential travel times and cross correlation, complete long period waveforms in a number of frequency bands, surface wave dispersion measurements (with 35 s – 150 s periods) and long period (150 s – 300 s) Love and Rayleigh wave dispersion measurements (Figure 3.1). This model incorporates the anisotropy of the mantle. The wave velocity predictions are reported as a deviation from Preliminary Reference Earth Model or PREM (Dziewonski and Anderson, 1981) velocities. The model predicts shear-wave velocities throughout the full extent of the mantle.

Ritzwoller et al. (2002) use scattering theory to create a tomographic map of S-wave velocities in the Earth (Figure 3.2). Rayleigh and Love wave group velocity measurements with periods between 20 s and 150 s were used to create both a diffraction tomography map and a traditional Gaussian tomography map (using ray theory). Diffraction tomography yields more detailed results for long periods and is especially

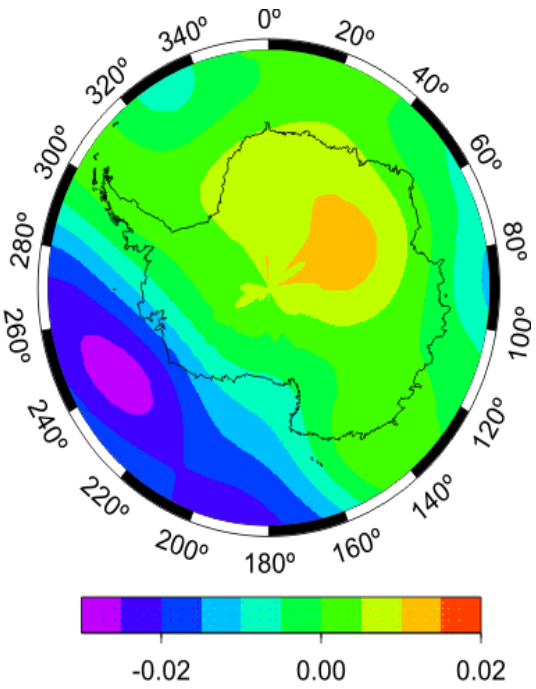

Figure 3.1: Seismic S-wave velocity fractional deviation from PREM ($\frac{Vs - V_{PREM}}{V_{PREM}}$) for model S20A (Ekstrom and Dziewonski, 1998) at a depth of 310 km.

helpful in imaging oceanic regions. In general, diffraction tomography produces larger velocity anomalies and thus it should also produce larger anomalies in mantle viscosity. Both the diffraction and ray theory methods yield velocities to a depth of 400 km.

3.3 Converting Seismic Velocities to Mantle Viscosity

By assuming that variations in seismic wave velocity are caused only by changes in temperature (and not composition) and that changes in temperature equate to changes in viscosity, we can use seismic tomography to create a map of mantle viscosity beneath Antarctica. The validity of this assumption can vary by location (Klosko et al., 2001, Wu et al., 1998). Following the method of Kaufmann et al. (2005), the viscosity

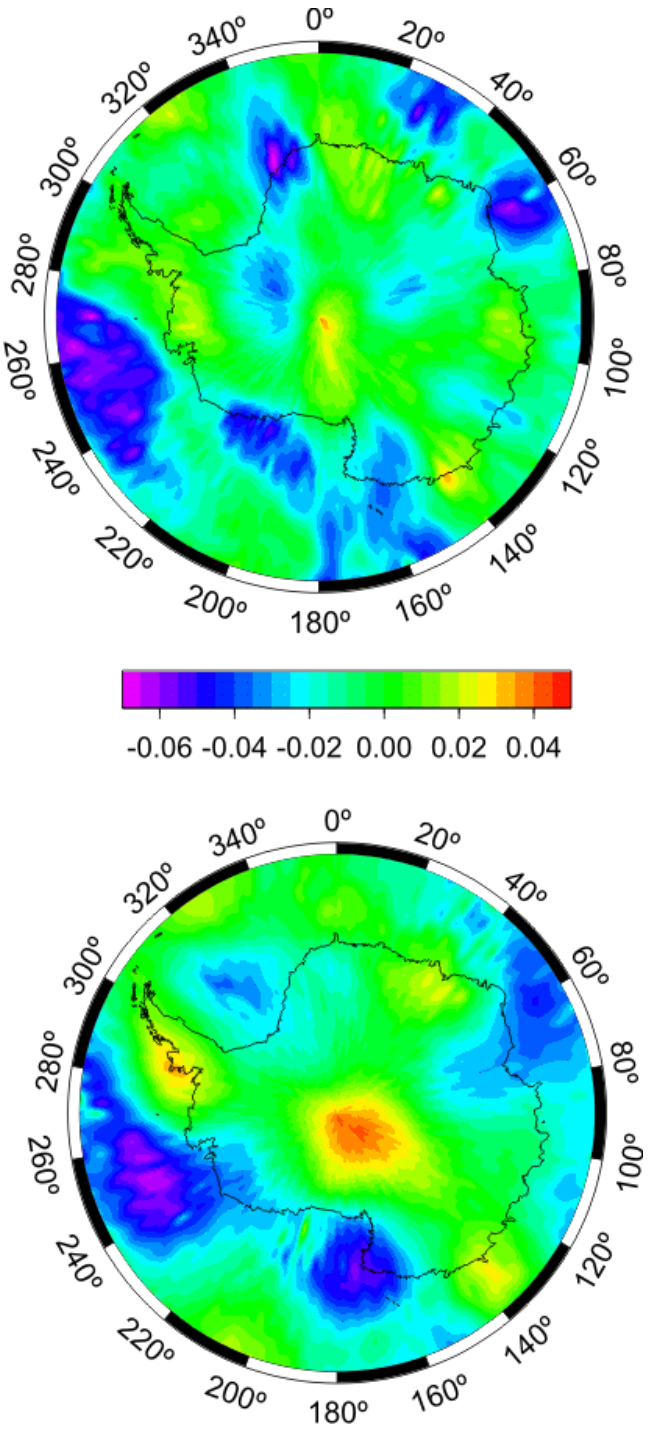

Figure 3.2: Seismic wave velocity fractional deviation from PREM at a depth of 310 km (Ritzwoller et al., 2002). (A) shows the results using ray theory and (B) shows the results using scattering theory.

perturbations can be determined through scaling the shear wave velocity anomalies as shown in Equation 3.3.

$$\Delta\eta = \exp\left(\frac{E + pV}{RT}\frac{1}{\alpha}\frac{1}{T_0^{\,2}}\frac{d\ln\rho}{d\ln v_s}d\ln v_s\right) \tag{3-3}$$

where ρ is the density, T is the temperature, T_0 is a radial reference temperature, v_s is the S-wave velocity, E is the activation energy, V is the activation volume, p is the pressure, R is the gas constant and α is the coefficient of thermal expansion and is equal to $\frac{1}{\rho}\left(\frac{\partial\rho}{\partial T}\right)_P$.

High temperature and high pressure experiments suggest that the value of (d ln ρ)/(d ln v_s) is approximately 0.3 (Chopelas and Boehler, 1992; Karato, 1993). Values for (E + pV)/R, α and T_0 with depth are given in Table 3.1. Temperature profiles for whole mantle convection and layered mantle convection are both available but the lateral viscosity variations obtained from the two are quite similar (Figure 3.3).

3.4 Antarctic Mantle Viscosities

Using the two tomographic models and the method described in the previous section, maps of mantle viscosity at various depths for Antarctica were created (Figures 3.4 and 3.5).

Table 3.1: Parameters for Velocity to Viscosity Conversion[4]

Depth (km)	(E+pV)/R (10^4 K)	α (10^{-5} K^{-1})	T_0 for Layered Mantle Convection (K)[5]	T_0 for Whole Mantle Convection (K)[6]
350	8.2	1.725	2088	1990
450	8.3	1.65	2069	2100
550	8.5	1.5	2100	2200
700	8.3	1.463	2300	2230
900	8.7	1.425	2500	2275
1200	9.35	1.3	2600	2296
1500	9.97	1.177	2650	2470
1800	10.6	1.05	2700	2530
2200	11.0	0.9	2675	2562
2600	11.4	0.75	2750	2530
2835	11.7	0.65	3250	2675

[4] Depth dependant parameters required for the seismic wave velocity to viscosity conversion (Ivins and Sammis, 1995).
[5] Temperatures for layered mantle convection from Tackley (1993).
[6] Temperatures for whole mantle convection from Leitch and Yuen (1989).

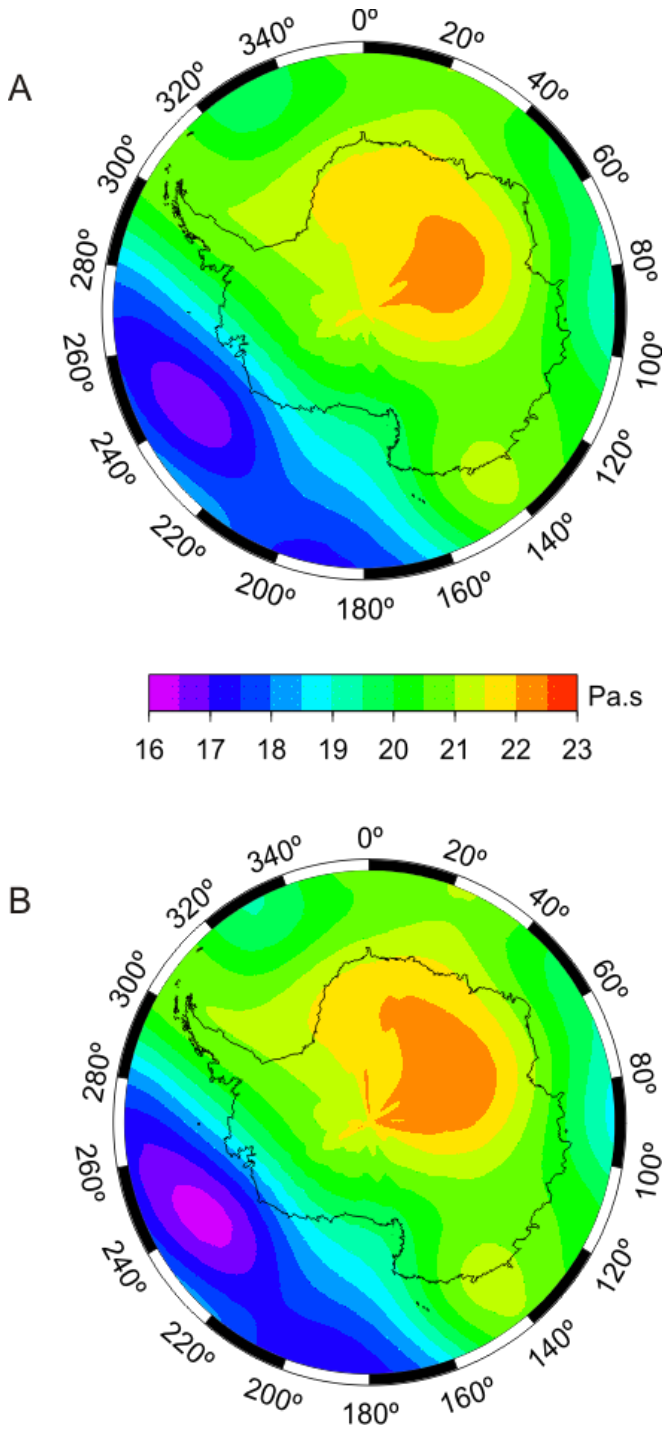

Figure 3.3: Mantle viscosities at a depth of 310 km, calculated here (Equation 3-3) using the S20A seismic tomographic model of Ekstrom and Dziewonski (1998). (A) shows the results using whole mantle convection and (B) shows the results using layered mantle convection.

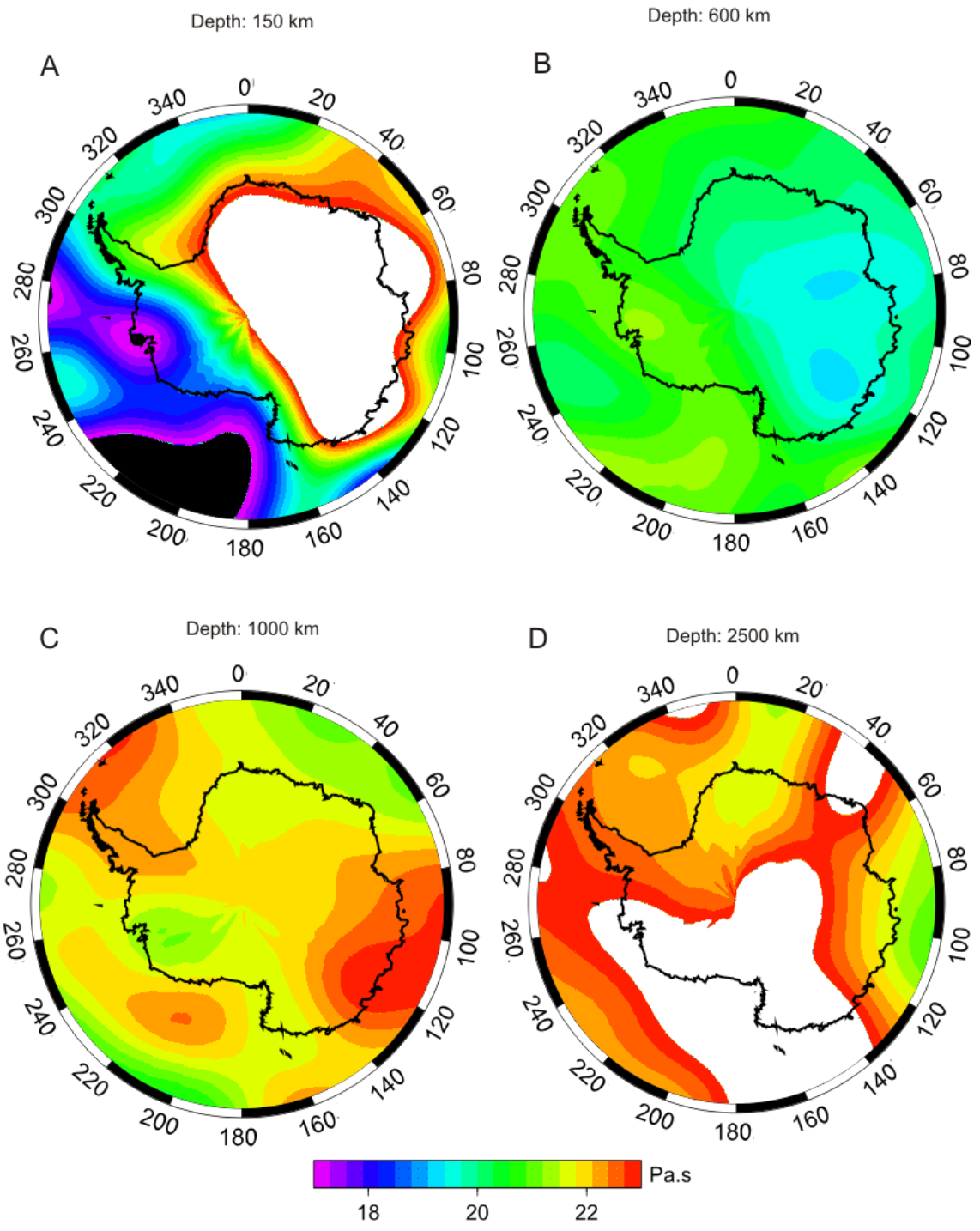

Figure 3.4: Mantle viscosity calculated using the S20A model of Ekstrom and Dziewonski (1998) and a layered Earth model at depths of (A) 150 km, (B) 600 km, (C) 1000 km and (D) 2500 km.

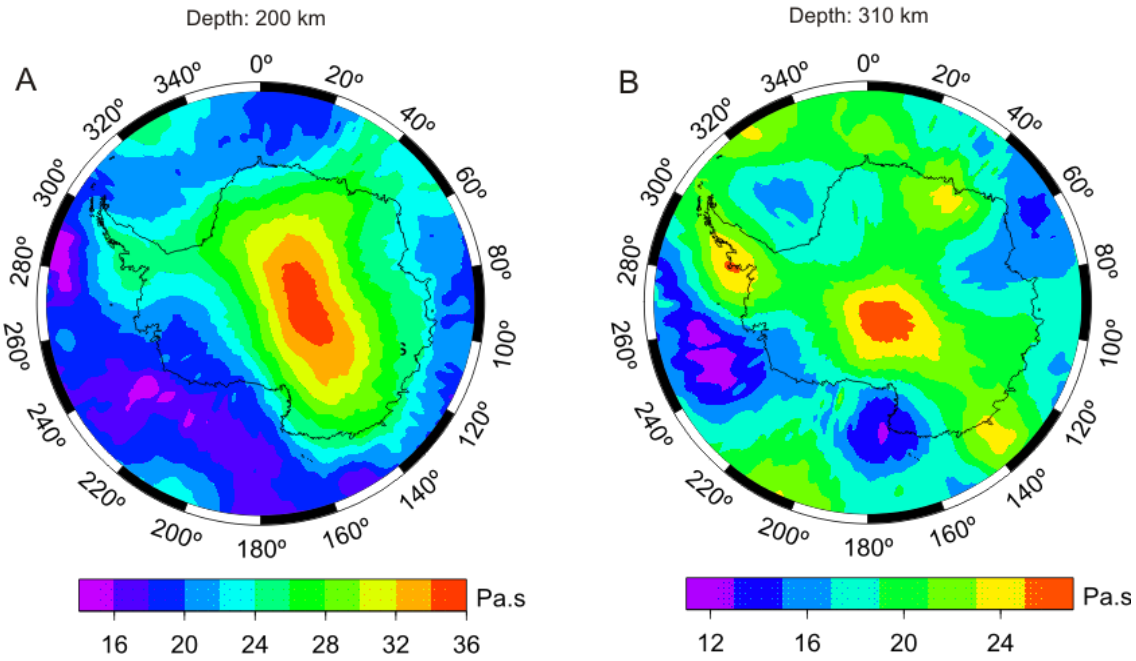

Figure 3.5: Mantle viscosity using wave velocities obtained from Ritzwoller et al. (2002) and assuming layered mantle convection at depths of (A) 200 km and (B) 310 km.

3.4.1 Discussion

The viscosity map obtained using S-wave velocities from S20A (Ekstrom and Dziewonski, 1998) conforms to expectations for mantle viscosity for Antarctica. At a given depth, S-wave velocities vary between -0.03 and 0.02, resulting in viscosities between 10^{16} Pa·s and 10^{23} Pa·s at 310 km (Figure 3.3). The cratonic nature of East Antarctica suggests that a high viscosity mantle should be present beneath it and we see this in the asthenosphere depth map. The West Antarctic Rift System underlies the part of West Antarctica adjacent to East Antarctica and defines a tectonic region that is substantially different from cratonic East Antarctica. This rift system is similar to the East Africa Rift and the Basin and Range, suggesting that West Antarctica should be situated above regions with lower asthenosphere viscosity.

S-wave velocities obtained from diffraction and ray methods using results from Ritzwoller et al. (2002) give a very different viscosity distribution (Figure 3.5). At 200 km depth, regions of high viscosity in East Antarctica and lower viscosities in West Antarctica appear, similar to S20A, but at 310 km they have disappeared. Variations in S-wave velocity are approximately double the variations (between -0.07 and 0.05) seen in S20A and thus the variations in viscosity become quite large giving viscosities that range from 10^{11} Pa·s to 10^{27} Pa·s at 310 km depth. These large variations in viscosity seem unlikely. Ivins and Sammis (1995) predict that mantle viscosity ranges laterally by about two orders of magnitude in the upper mantle (below 350 km) and three orders of magnitude above 350 km depth. Forte and Mitrovica (2001) use geodynamic and seismic data to infer that lateral variations in the mantle likely have a three order-of-magnitude range. Additionally, the pattern of high and low viscosity regions is similar to the pattern seen with S20A at 200 km depth but at 310 km it changes. At 310 km depth the region of high viscosity shifts towards West Antarctica and several regions of East Antarctica experience very low viscosities unlike expected values for this cratonic region.

Two possible reasons exist that could explain the discrepancy between the two results. The first is low resolution seismic wave velocity data in the region. Antarctica suffers from low resolution in the data that may not be present in other regions on Earth. Resolution for most of the continent is estimated at 625 km to 775 km for long period waves (150 s) where optimal resolution (of 333 km) usually only occurs for short periods. It is also possible that the assumption that lateral variations in mantle viscosity are largely temperature dependent is incorrect. Variations caused by compositional variations and anisotropic effects could have a significant impact on the seismic wave velocities seen

but they are not accounted for using the method of conversion from wave velocity to viscosity discussed above. For instance, if 50% of wave velocity variations are assumed to be compositional the viscosity values obtained from Ritzwoller et al. (2002) range from 10^{15} Pa·s to 10^{22} Pa·s at 310 km depth. This implies that at least 50% of the wave velocity variations in the study (if not more) are due to mantle composition and not temperature.

3.4.2 Comparison to the Basin and Range

Both the Basin and Range region of North America and the West Antarctic Rift System experienced wide-spread rifting leaving an area of thinned crust after approximately 200 km of extension. Active volcanism is seen in both areas. The Basin and Range and the West Antarctic Rift System may both still be experiencing rifting at rates of 2 – 3 mm/yr (Dietrich et al., 2004, van Wijk et al., 2008). These similarities lead us to believe that asthenosphere viscosities in West Antarctica should be close to those observed at Lake Bonneville and Lake Lahontan. In Lake Bonneville, in the Basin and Range area, asthenosphere viscosities range between 10^{17} Pa·s and 2×10^{20} Pa·s while at nearby Lake Lahontan modelled viscosities have a minimum value of 5×10^{17} Pa·s (Bills et al., 1994 and Bills et al., 2007). Shallow mantle viscosities in the range of around 10^{17} Pa s to 10^{20} Pa s may be appropriate for West Antarctica. This agrees with the viscosity results obtained through the seismic tomography of S20A as found above.

3.5 Summary

Analysis of seismic wave tomography can be used to create a map of mantle viscosity beneath Antarctica by assuming that changes in wave velocity indicate changes in temperature and changes in temperature lead to changes in viscosity. The results for

the S20A model (Ekstrom and Dziewonski, 1998) give a viscosity distribution in Antarctica that is what we would expect to see including low viscosity regions beneath West Antarctica and higher viscosities beneath East Antarctica, particularly in the asthenosphere. Results from the Ritzwoller et al. (2002) tomography yield a range of viscosities is much larger than expected and the regions of high and low viscosity do not always agree with expectations. If the Ritzwoller et al. (2002) seismic tomographic results are confirmed in future studies, this would strongly suggest that some of the lateral variation is due to compositional differences and not only lateral variations in temperature. In Chapter 5, the S20A model results will used as a physically plausible model of Antarctic mantle viscosity and a starting point in comparing vertical crustal motion rates given by glacial isostatic adjustment models to rates given by GPS observations.

Chapter 4 – Comparing Lithosphere Thickness and Elevation

4.1 Overview

Mountain belts are frequently created by continental or island-arc collisions, resulting in thickened crust. This implies that the increased elevation of the crust is supported by a thick crustal root. This is the case in some areas (e.g. the Himalayas). Seismic structure data indicate, however, that in other regions, such as the North American Cordillera, no crustal root is present (Hyndman, 2010). Here, the crustal thickness is 35 km, slightly thinner than the 40 km average found in lower elevation, stable regions. The high elevation of this thin crust can be explained by hotter mantle in that area. In other words, the mountain belts are supported by thermal expansion of the asthenosphere.

By this argument, an examination of the crustal thickness and the topographic elevation of a region will indicate whether the underlying mantle is anomalously hot or cold. This interpretation can then be checked through temperatures inferred from geothermal heat flow and upper crust radioactive heat generation, temperature-controlled seismic velocities from shear wave tomography, and temperature depths from mantle xenoliths obtained on cratons. These temperatures can also be related to effective elastic thickness of the lithosphere as it is controlled by the temperature-controlled depth of the brittle-ductile transition.

Hyndman (2010) and Hyndman and Currie (2011) analyzed elevation and crustal thickness for the North American Cordillera (Figure 4.1). It can be seen that

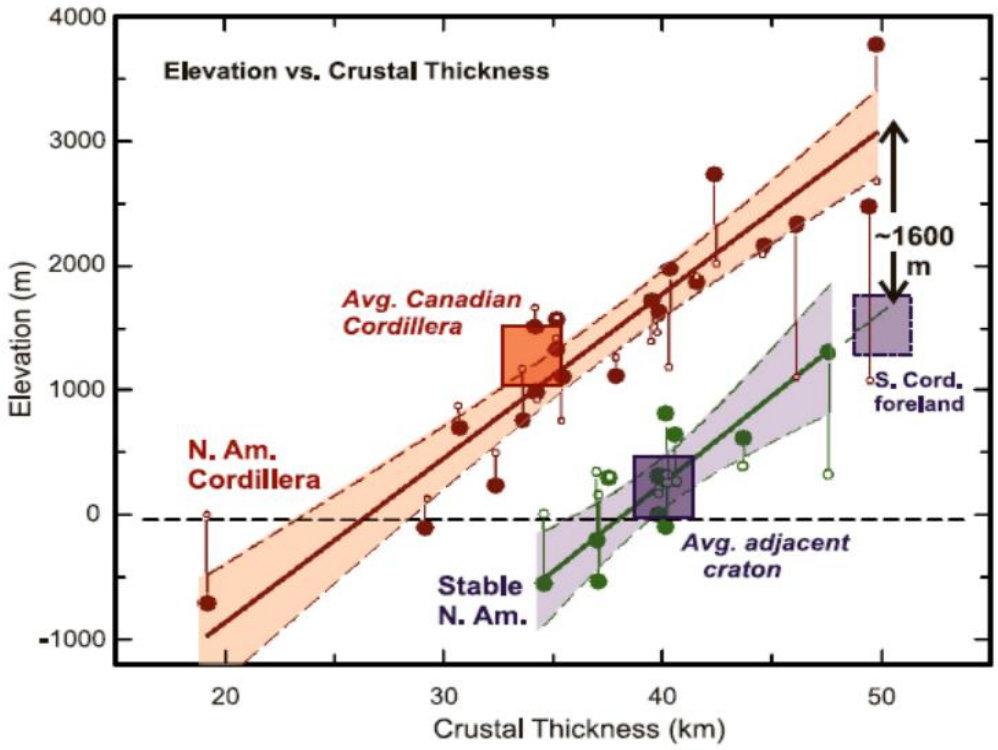

Figure 4.1: Relationship between elevation and crustal thickness for the North American Cordillera. Open symbols have not been corrected for density while solid symbols have. Boxes represent the averages for the Cordillera and the craton (Hyndman, 2010).

cold stable areas occupy a different region of the graph from hot backarc regions and the two regions have separate best-fitting linear regressions. A similar analysis for Antarctica could suggest whether different parts of Antarctica are located over high or low temperature mantle that may, in turn, relate to its viscosity.

4.2 Crustal Thickness and Elevation Using BEDMAP and CRUST 2.0

Using CRUST 2.0 (Bassin et al., 2000; Mooney et al., 1998) to obtain crustal thicknesses and BEDMAP (Lythe and Vaughan, 2001) to obtain elevations, an Antarctic-wide analysis similar to that of Hyndman (2010) was carried out.

CRUST 2.0 (Bassin et al., 2000) gives world wide crustal thicknesses on a 2° × 2° grid (Figure 4.2). The thicknesses are based on seismic refraction data published between 1948 and 1995. CRUST 2.0 is an update of CRUST 5.1 (Mooney et al., 1998). Most of the seismic refraction profiles were observed in the northern hemisphere and in a few, select southern hemisphere countries as well. Antarctica in particular is quite sparsely sampled, with roughly 15 refraction profiles obtained on the continent, most of which are found along the Weddell Sea.

BEDMAP (Lythe and Vaughan, 2001) is a database of elevation and ice thickness measurements taken throughout Antarctica. The data are quite well constrained in West Antarctica but sparse in some areas of East Antarctica.

The elevations obtained from BEDMAP were corrected for crustal density according to Hasterok and Chapman (2007) using equation 4-1.

$$\Delta\varepsilon_C = h'_C\left(1-\frac{\rho'_C}{\rho_M}\right)-h_C\left(1-\frac{\rho_C}{\rho_M}\right) \tag{4-1}$$

where $\Delta\varepsilon_C$ is the change in correction in elevation, h'_C is the standard crustal thickness of 39 km, ρ'_C is the standard crustal density of 2850 kg/m^3, ρ_M is the mantle density of 3300 kg/m^3, and h_C and ρ_C are the crustal thickness and crustal density at the location of the elevation measurement respectively. To get the corrected elevation the correction is added to the observed elevation.

A correction for ice loading was made using vertical displacements computed using the GIA model of Ivins and James (2005). The vertical displacements (negative downwards) were subtracted from the elevation to correct for the depression of the Earth's crust caused by ice sheet surface loading.

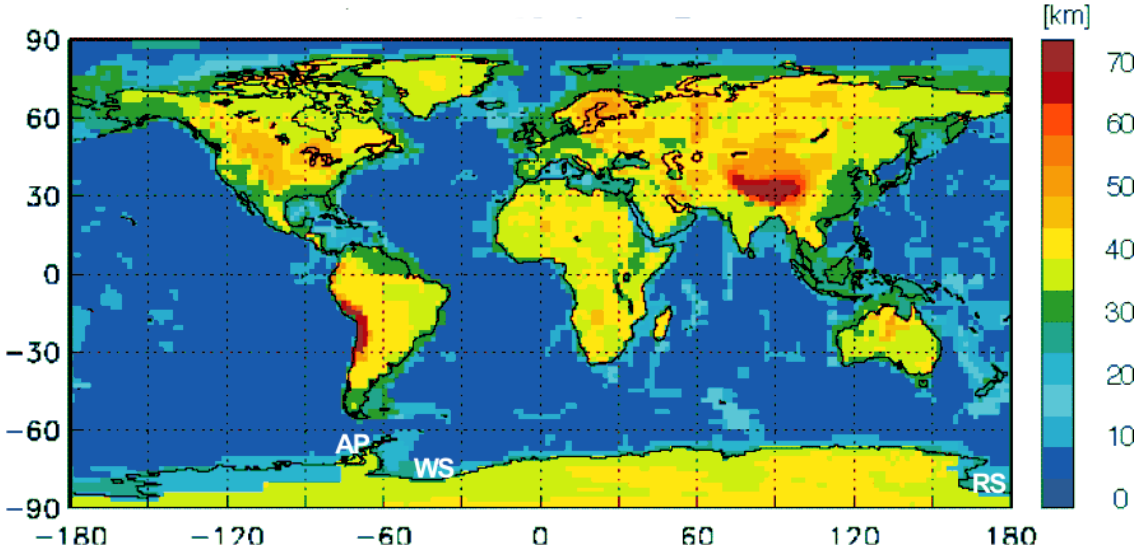

Figure 4.2: Crustal thickness of the world as found by Bassin et al. 2000. Continental crustal thicknesses in East and West Antarctica range between 35 km and 45 km (WS – Weddell Sea, RS – Ross Sea, AP – Antarctic Peninsula).

For this study, Antarctica was divided into six regions (Figure 4.3 top). East Antarctica is cratonic and thus expected to have a thick crust. The Antarctic Peninsula includes regions of active tectonics along the border of the Antarctic Plate. Ellsworth Land contains the Ellsworth Mountains and is largely a high plateau. Marie Byrd Land contains an area of domal uplift possibly caused by a hot spot beneath the region. The Transantarctic Mountains are a mountainous area through the middle of the continent where West Antarctica and East Antarctica meet. The West Antarctic Rift System is a region of failed continental rifting leaving behind thinned crust.

Crustal thicknesses and elevations, keyed by the regions, are shown in Figure 4.3 (bottom). Considering the data in its entirety, a weak trend of increasing crustal

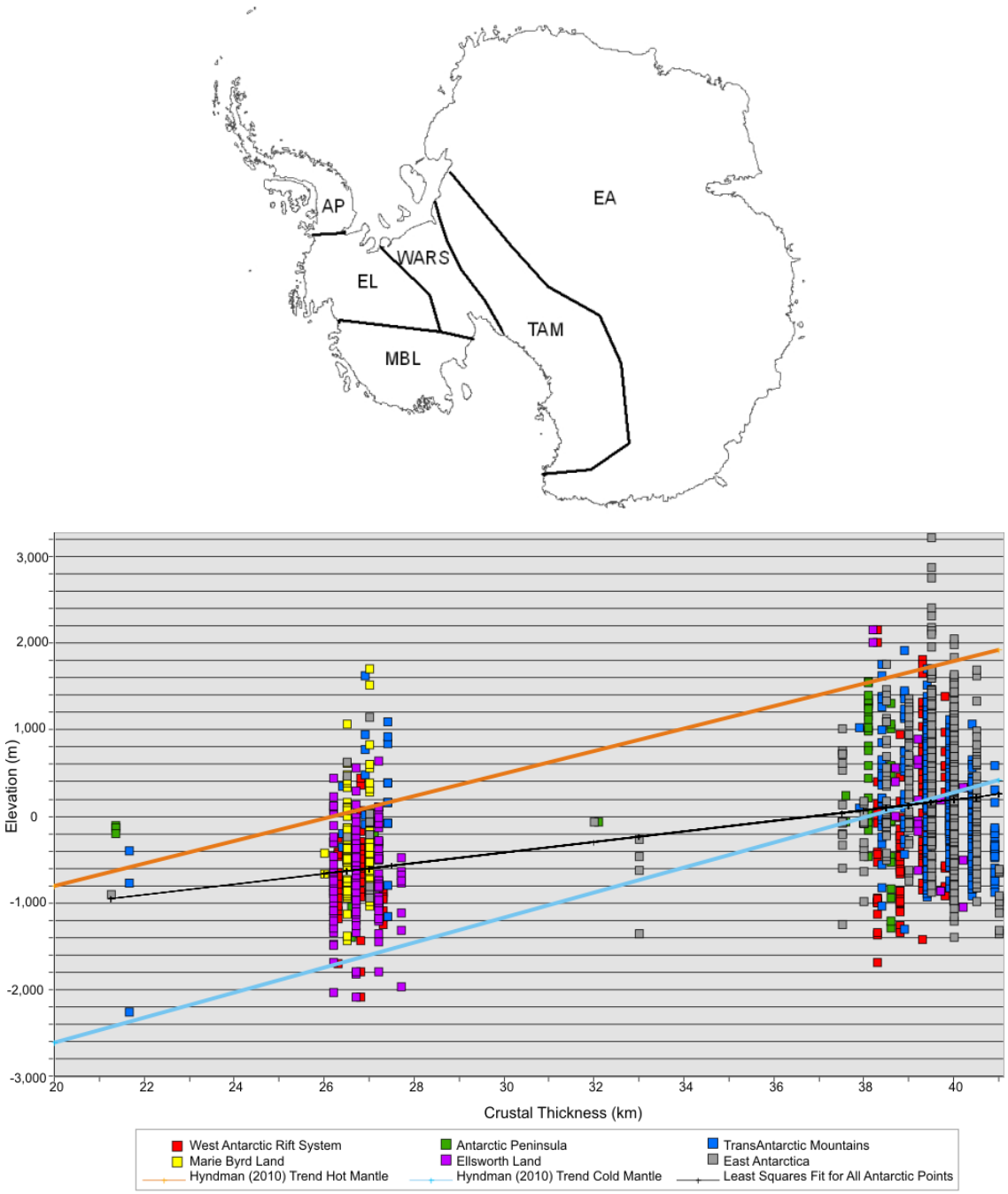

Figure 4.3: (Top) Map of the regions of Antarctica (AP – Antarctic Peninsula, EA – East Antarctica, EL – Ellsworth Land, MBL – Marie Byrd Land, TAM – TransAntarctic Mountains, WARS – West Antarctic Rift System). (Bottom) Elevation versus crustal thickness for Antarctic regions using crustal thicknesses from CRUST 2.0 (Bassin et al., 2000) and bed elevations from BEDMAP (Lythe and Vaughan, 2001). The black line is a linear regression through all the data. The red and blue lines are the regression found by Hyndman (2010) corresponding to hot backarc regions and cold cratonic regions, respectively.

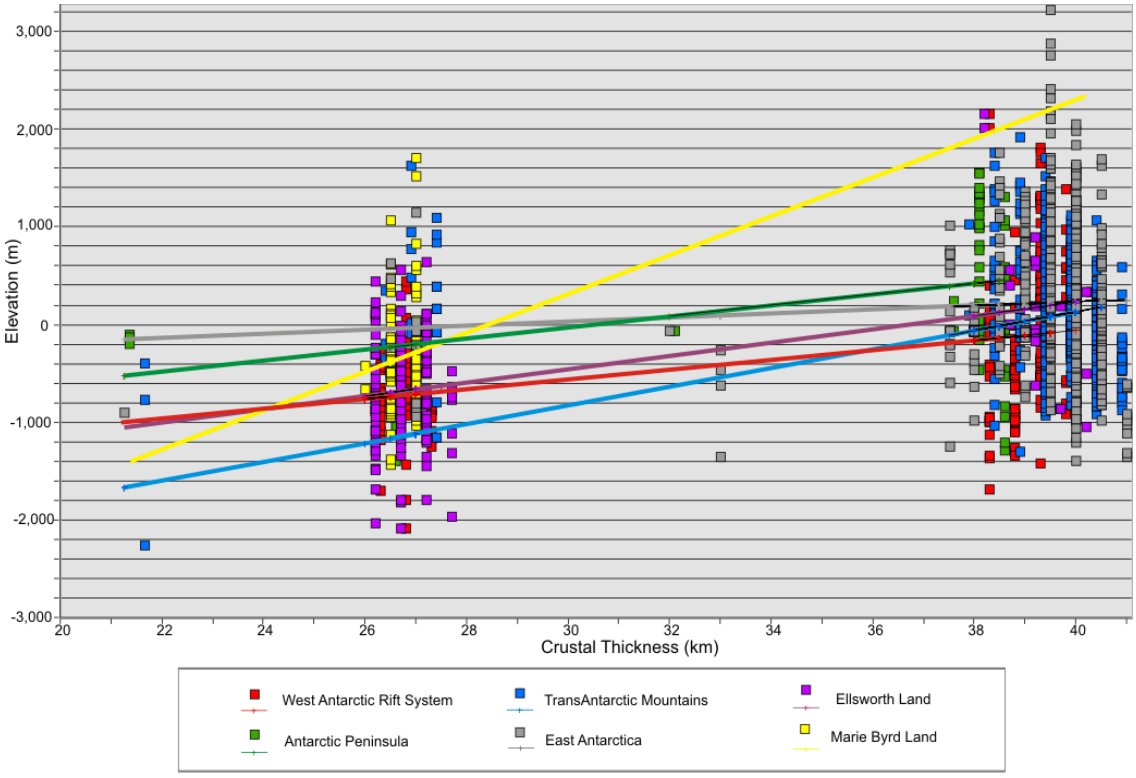

Figure 4.4: Elevation versus crustal thickness for Antarctic regions using crustal thicknesses from CRUST 2.0 (Bassin et al., 2000) and bedrock elevations from BEDMAP (Lythe and Vaughan, 2001). Linear regression lines are shown for each region.

thickness with bedrock elevation is visible but there is no obvious separation of the data into two separate trends corresponding to hot and cold mantle.

Individual linear regression lines for each region are shown in Figure 4.4. The regressions generally indicate increasing crustal thickness with bedrock elevation for each region, but the postulated grouping into hot mantle and cold mantle regions is not present. For example, the East Antarctic trend line lies above most of the other trend

lines, yet the expectation would be that the East Antarctic trend line would like below most of the others.

The analysis of the average crustal thicknesses and elevations by region indicates the affinity of different regions Antarctica with cold cratonic mantle and hot backarc mantle. The average elevation and crustal thickness for each region and the Hyndman (2010) best fit lines are shown in Figure 4.5. The average for the East Antarctic craton falls on the cold mantle line as expected. Marie Byrd Land, being the location of a possible hotspot, is a region where hot mantle is expected and results here concur with that. Nearby Ellsworth Land also falls nearest to the hot mantle line confirming our expectations for West Antarctica. The West Antarctic Rift System average lies closest to the cold mantle trend which is not what we would expect to see. The CRUST 2.0 crustal thickness map (Bassin et al., 2000) shows an extrapolated crustal thickness in the area of 35 km. It could be that this extrapolation was based on sparse data particularly as none of the reflection profiles used came from West Antarctica. Seismic wave studies performed in the Ross Sea (a region which is part of the West Antarctic Rift System) show much lower crustal thicknesses than found in the CRUST 2.0 data. Cooper et al. (1997) and Cooper et al. (1987) interpret the thickness of the crust to be between 17 km and 20 km in Victoria Land Basin and Central Basin of the Ross Sea. The Antarctic Peninsula lies midway between hot and cold mantle suggesting that modest amounts of asthenospheric support are present but not as much as is seen in backarc regions. Standard deviations on the averages are quite high typically ranging from 600 m to 800 m for the elevation and 1 km to 5 km in the crustal thickness. To pursue this analysis further, the next section will focus on smaller scale, precise crustal thickness studies in various regions in Antarctica.

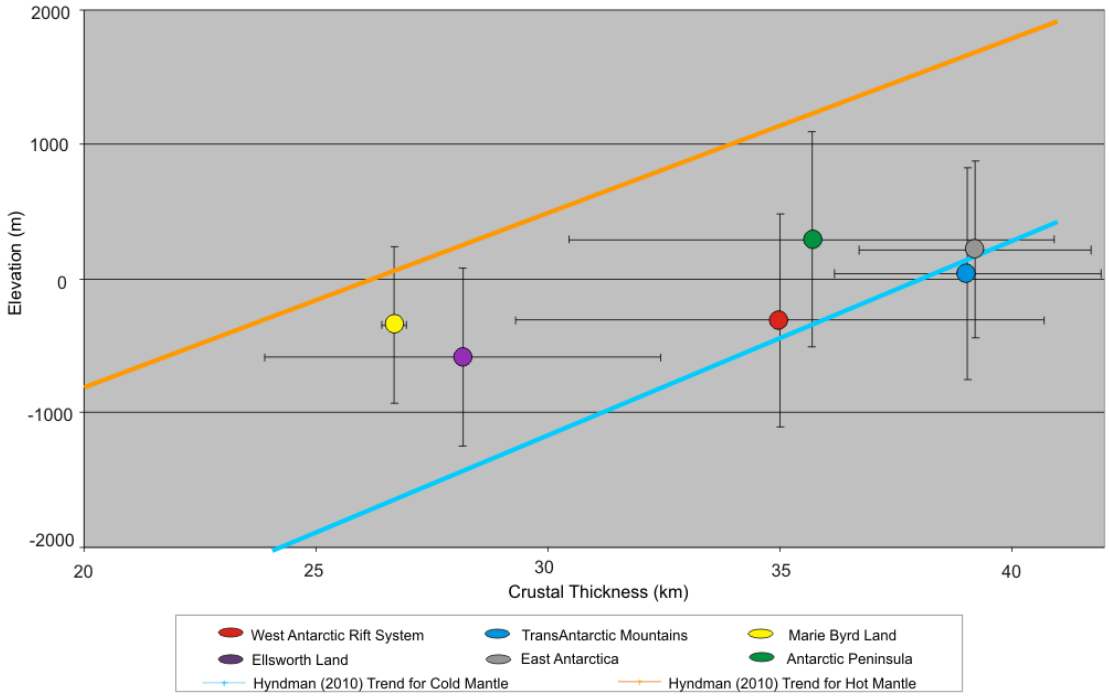

Figure 4.5: The average values of elevation and crustal thickness for Antarctic regions using crustal thicknesses from CRUST 2.0 (Bassin et al., 2000) and bed elevations from BEDMAP (Lythe and Vaughan, 2001).

4.3 Crustal Thickness and Elevation Using Localized Crustal Thickness Studies

Several studies provide more precise measurements of crustal thickness in localized areas of Antarctica (Winberry and Anandakrishnan, 2004, Leitchenkov et al., 2008, Bayer et al., 2009, Isanina et al., 2009). Winberry and Anandakrishan (2004) and Bayer et al. (2009) calculate crustal thickness using teleseismic earthquakes and receiver functions in Marie Byrd Land and Dronning Maud Land, East Antarctica respectively. Reflections and refractions of seismic waves are used to model the depth to various interfaces including the base of the crust. Reflection and refraction arrivals were also

recorded by Leitchenkov et al. (2008) through the use of sonobuoys at sites just offshore from Dronning Maud Land. At Lake Vostok in East Antarctica, Isanina et al. (2009) made observations of seismic waves at three points around the lake and used the earthquake converted–wave method to determine the structure of the crust and mantle beneath.

Using the crustal thickness observations obtained from these studies and bedrock elevations from BEDMAP (Lythe and Vaughan, 2001), an analysis similar to the last section was performed. Figure 4.6 (top) shows the location of each data point. Figure 4.6 (bottom) shows the elevations plotted against crustal thicknesses, the points corresponding to the average value for each study, and the two trends inferred by Hyndman (2010). The West Antarctic average shows evidence of a hot mantle as it lies slightly closer to the Hyndman (2010) trend for hot mantle. The average of the East Antarctic data falls on the Hyndman (2010) best fit line for cold mantle, as would be expected for a cratonic region.

The West Antarctic data were largely obtained from Marie Byrd Land and (as in the previous section) the average of these observations lies quite close to the hot mantle regression line. This implies that Marie Byrd Land likely lies above a hot mantle region just as the North American Cordillera does. Two of the East Antarctic studies (Bayer et al., 2009 and Isanina et al., 2009) see average crustal thickness and elevation data that lie directly on the cold mantle regression line. This indicates the East Antarctica is cratonic and has similar crustal thickness and elevation to the North American Craton. The average of the third East Antarctic study (Leitchenkov et al., 2008) lies between the two

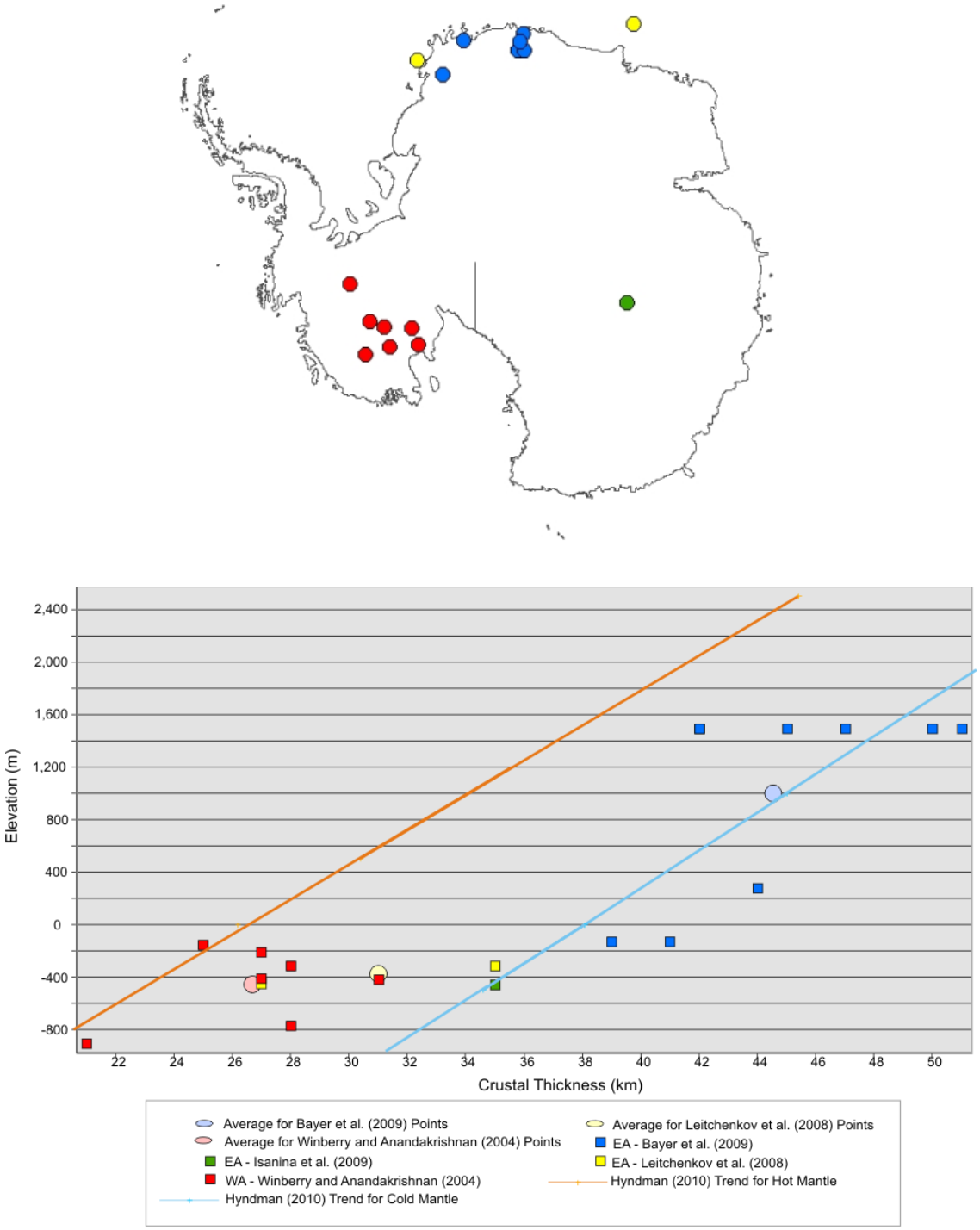

Figure 4.6: (Top) Map of the study regions. (Bottom) Elevation versus crustal thickness for Antarctic regions using crustal thicknesses from Winberry and Anandakrishnan (2004), Leitchenkov et al. (2008), Bayer et al. (2009) and Isanina et al. (2009) with bed elevations from BEDMAP (Lythe and Vaughan, 2001) (EA – East Antarctica, WA – West Antarctica). Symbols are consistently colour coded.

trends. This study was undertaken offshore and may include crust transitional from continental to oceanic. Standard deviations on the averages remain quite high in this analysis with elevation deviations ranging from 100 m to 750 m and crustal thickness ones between 1 km and 5 km.

4.4 Summary

The available continent-wide information on crustal thicknesses (Bassin et al., 2000) and bedrock elevations (Lythe et al., 2001) for Antarctica do not establish separate trends of hot and cold mantle, as was done for the North American Cordillera and craton (Hyndman, 2010). Average values for most regions, do, however, exhibit an affinity for either the cold or hot mantle trends. For example, the East Antarctic data falls on the Hyndman (2010) fit for cold mantle areas while Marie Byrd Land and Ellsworth Land fall on the fit for hot mantle. Other regions lie between the two trends. The West Antarctic rift system is anomalous because it falls on the cold mantle trend but crustal thicknesses of 35 km are unusually large for a region where geologically-recent rifting has occurred. With the exception of the WARS, the results agree with the expectations from the seismic wave analysis performed in Chapter 3.

In the more localized studies of crustal thickness the West Antarctic data fall near to the hot mantle trend found in North America while the East Antarctic data fall on the cold mantle fit. These results also agree with the results found in Chapter 3 where S20A seismic wave velocities were converted to viscosity. This hot mantle seen in West Antarctica indicates lower viscosities in the mantle while cold mantle beneath East Antarctica indicates higher viscosities. To determine the hot and cold mantle trends for

bedrock elevation and crustal thickness for Antarctica, as was done in North America, further observations of crustal thickness would be required.

Chapter 5 – Comparing GPS Observations to Glacial Isostatic Adjustment Uplift Predictions

5.1 Overview

Loaded by fluctuating ice sheets, Antarctica is a continent that is continually changing. As the ice sheets change by flow into the oceans and by melting, rebound occurs in the lithosphere at rates that depend on the mantle viscosity and on changes to the thickness of the ice. Postglacial rebound (PGR) or glacial isostatic adjustment (GIA) models of this vertical crustal motion have been proposed and revised for many years but only recently have GPS crustal uplift data been available to compare to model predictions. Bevis et al. (2009) describe new GPS observations of crustal uplift in Antarctica and compare the results to GIA model predictions, including the IJ05 model of Ivins and James (2005). Predicted uplift rates based on the IJ05 loading history have, to date, been based on a small number of different Earth models but many other possible Earth model (viscosity) combinations can be examined. By systematically varying the viscosity in the asthenosphere, transition zone and lower mantle, the IJ05 Earth models that best fit the GPS data can be determined using a χ^2 measure of goodness-of-fit.

5.2 Glacial Isostatic Adjustment Modelling

With a given mantle viscosity profile and a given ice history, present-day vertical crustal motion caused by glacial isostatic adjustment can be predicted.

The Earth can be approximated as having a layered rheology so the Earth models used here contain spherically symmetric layers with uniform density, viscosity and elastic properties. The crustal motion response is calculated using the ice history described in Chapter 1 (termed the IJ05 ice model for GIA calculations; Ivins and James, 2005) and

the methods of James and Ivins (1998). For a spherically symmetric load (e.g, a spherical cap), the response is a Legendre function where each degree n corresponds to a discrete wavelength and has its own characteristic set of decay times and associated responses. The response can also be represented with Love numbers (Farrell, 1972; Peltier, 1974) where the Love numbers are defined by the boundary conditions used in the model. A viscoelastic Love number is made up of a viscous and elastic component and they also depend on Legendre degree. The response is calculated as follows:

$$\begin{bmatrix} U_n(r) \\ V_n(r) \\ \Phi_{2,n}(r) \end{bmatrix} = \frac{ag_0}{m_e} \begin{bmatrix} h_n(r)/g_0 \\ l_n(r)/g_0 \\ -k_n(r) \end{bmatrix} \quad (5\text{-}1)$$

where U_n, V_n and $\Phi_{2,n}$ are the vertical displacement, horizontal displacement and gravitational potential due to the deformation, r is the distance from the centre of the Earth, a is the Earth's radius, g_0 is the initial gravitational acceleration, m_e is the mass of the Earth and h_n, l_n and k_n are Love numbers (Peltier, 1985).

Predicted crustal motion responses were calculated for a wide range of viscosities using a three layer (asthenosphere, transition zone and lower mantle) Earth model. Asthenosphere viscosities ranged between 10^{16} Pa·s and 10^{22} Pa·s, transition zone viscosities between 10^{16} Pa·s and 2 x 10^{23} Pa·s and lower mantle viscosities between 10^{19} Pa·s and 10^{26} Pa·s. The lithosphere thickness used was a relatively thin 40 km, as only GPS observations from West Antarctica were utilized in this thesis.

5.3 GPS Observations

The significant ice cover, remote location, and challenging environmental conditions in Antarctica makes setting up GPS stations more difficult than in any other part of the world. Between 2001 and 2006 a network of GPS stations was installed in

West Antarctica on 18 bedrock outcrops (the West Antarctic GPS network or WAGN). The majority of the stations have two survey markers and crustal motion has been measured at each. Bevis et al. (2009) published crustal motion rates (vertical rates shown in Table 5.1) from the 12 WAGN stations which have been active for 3 or more years, as well as several stations in East Antarctica and the Antarctic Peninsula.

5.3.1 Station Locations

GPS observed crustal motion rates are available for 12 locations in West Antarctica and the Transantarctic Mountains, 4 locations in the Antarctic Peninsula and 6 locations in East Antarctica (Figure 5.1). Only the West Antarctic and Antarctic Peninsula stations were used in this study because East Antarctica is only sparsely populated with GPS stations, all of which are located on the coastline.

5.3.2 Reference Frame Analysis

In order for comparisons to be made between observed GPS vertical velocities and predicted GIA model uplifts we must ensure that they are in the same reference frame. Geodetic reference frames provide coordinates for a number of points around the planet. Movements related to plate tectonics, subsidence or any number of other changes can be recorded relative to these stations. With a consistent reference frame, comparisons between various sets of data become much simpler even if the data are from different locations. The coordinates are calculated most commonly through four different geodetic methods: GPS, VLBI, SLR and DORIS. The network of these four systems is continually changing and thus terrestrial reference frames must be updated regularly (Altamimi et al., 2001, Altamimi et al., 2005, Altamimi and Collilieux, 2008).

Table 5.1: Vertical Crustal Motion Rates from Bevis et al. (2009)[7]

Station	Latitude (degrees)	Longitude (degrees)	Uplift Rate (mm/yr)	Uncertainty in Uplift Rate (mm/yr)
DAV1	-68.58	77.97	-1.4	0.2
DAVR	-68.58	77.97	-0.9	0.7
DUM1	-66.67	140.00	-1.5	0.2
MAW1	-67.60	62.87	-0.8	0.2
SYOG	-69.01	39.58	0.6	0.2
VESL	-71.67	-2.84	1.3	0.3
CAS1	-66.28	110.52	0.5	0.2
OHIG	-63.32	-57.90	7.6	1.0
OHI2	-63.32	-57.90	7.0	0.7
OHI3	-63.32	-57.90	6.5	0.8
PALM	-64.78	-64.05	4.8	0.3
SPPT	-64.29	-61.05	7.5	1.8
MCM4	-77.84	166.67	-2.1	0.4
SCTB	-77.85	166.76	1.1	1.0
W01A	-87.42	-149.43	-4.3	0.8
W01B	-87.42	-149.44	-3.4	0.7
W02A	-85.61	-68.56	0.5	1.5
W02B	-85.61	-68.56	-3.2	1.2
W03A	-81.58	-28.40	-1.9	1.4
W03B	-81.58	-28.40	-1.1	1.2
W04A	-82.86	-53.20	1.6	1.8
W04B	-82.86	-53.20	3.9	0.8
W05A	-80.04	-80.56	4.0	1.0
W05B	-80.04	-80.56	3.9	1.8
W06A	-79.63	-91.28	-4.1	2.3
W07A	-80.32	-81.43	5.6	1.4
W07B	-80.32	-81.54	5.7	1.5
W08A	-75.28	-72.18	4.5	1.5
W09A	-82.68	-104.40	6.3	1.3
W12A	-78.03	-155.02	7.2	0.8
MBL1	-78.03	-155.02	4.9	1.0
HAAG	-77.04	-78.29	7.8	0.5

[7] Published uplift rates from the GPS observations published in Bevis et al. (2009). The first 7 stations are located in East Antarctica (DAV1, DAVR, DUM1, MAW1, SYOG, VESL and CAS1), the following 5 are in the Antarctic Peninsula (OHIG, OHI2, OHI3, PALM, SPPT) and the remaining stations are located in West Antarctica.

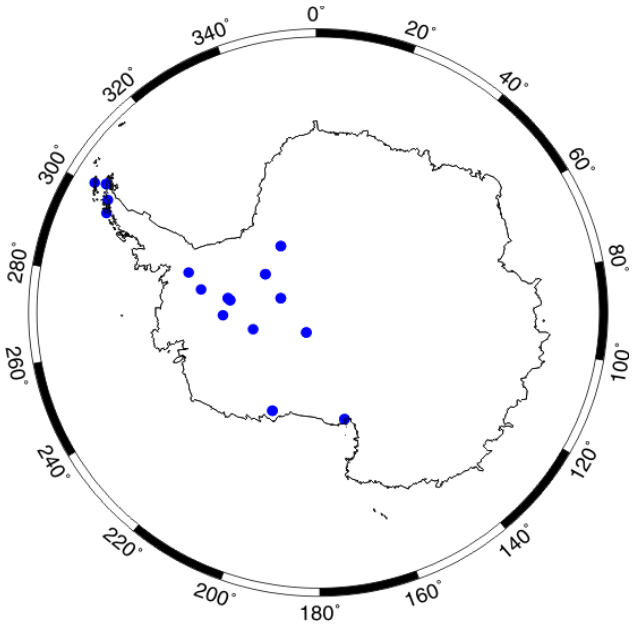

Figure 5.1: GPS stations currently reporting in Antarctica as part of the West Antarctic GPS Network (Bevis et al., 2009).

The global geodetic reference frame is provided by the International Terrestrial Reference Frame (ITRF); solutions for ITRF have been most recently published in 2000, 2005 and 2008. Measurements in one reference frame can be transferred into an updated one with the use of 14 transformation parameters (Table 5.2). All ITRF models provide positions and velocities at a number of stations around the world.

The Bevis et al. (2009) velocities were generated in a global frame in which horizontal velocities were minimized for 11 CGPS stations on the Antarctic plate and vertical velocities were minimized for 202 GPS stations located between 60°S and 60°N where net vertical velocity is expected to be zero. To clarify the Bevis et al. (2009) reference frame, a comparison was made between ITRF velocities and Bevis et al. (2009) velocities (Figure 5.2). The intercept for a line of best fit (with slope of 1) was calculated

for each comparison. The Bevis et al. (2009) velocities show a stronger correlation with the ITRF2005 observations, giving a RMS scatter of 3.0 mm/yr versus 3.7 mm/yr for the ITRF2000 observations, and analysis shows that the difference between the two intercepts (Bevis et al. (2009) vs. ITRF2005 and Bevis et al. (2009) vs. ITRF2000) is comparable to the difference between the two reference frames released at the time of publication of ITRF2005. Subtracting the ITRF2005 intercept from the ITRF2000 vertical velocity gives -2.1 mm/yr which is comparable to the published Z translation rate between the models (-1.8 mm/yr) within the ITRF Z translation uncertainty of 0.3 mm/yr (Figure 5.2).

Table 5.2: Parameters for transforming from ITRF2000 to ITRF2005[8]

Parameter	T1 (mm)	T2 (mm)	T3 (mm)	D (10-9)	R1 (mas)	R2 (mas)	R3 (mas)
Displacement	0.1	-0.8	-5.8	0.40	0.000	0.000	0.000
Uncertainty ±	0.3	0.3	0.3	0.05	0.012	0.012	0.012
Rates (yr^{-1})	-0.2	0.1	-1.8	0.08	0.000	0.000	0.000
Uncertainty ±	0.3	0.3	0.3	0.05	0.012	0.012	0.012

[8] T1, T2 and T3 are translational parameters while R1, R2 and R3 are the rotational ones. D is change to scale. The uncertainties are displayed below each value.

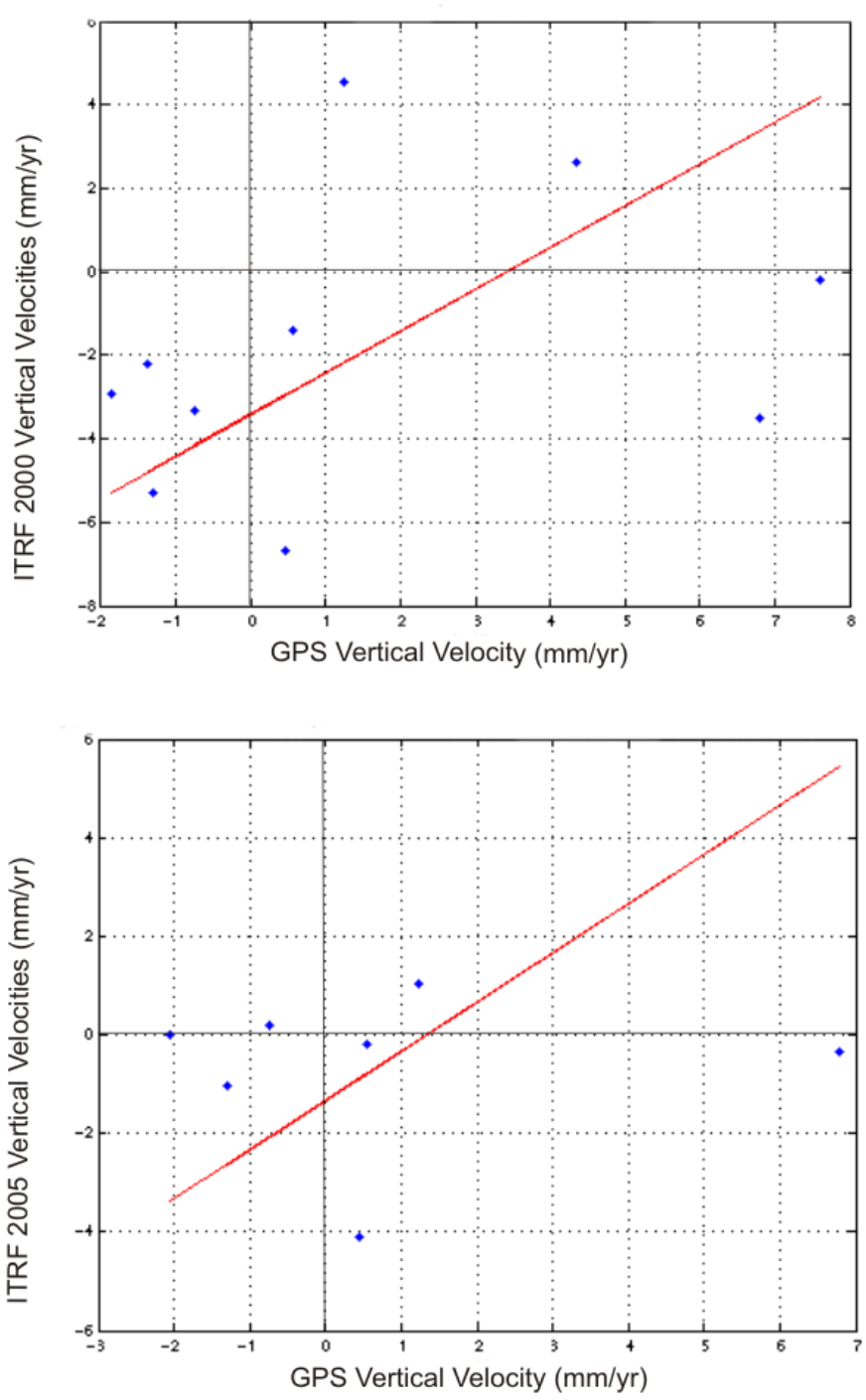

Figure 5.2: (Top) Comparison between ITRF2000 vertical velocities and those obtained in Bevis et al., 2009. Intercept occurs at -3.4 mm/yr with an uncertainty of 4.3 mm/yr. RMS scatter is 3.7 mm/yr. (Bottom) Comparison between ITRF2005 vertical velocities and those observed by Bevis et al., 2009. Intercept occurs at -1.3 mm/yr with an uncertainty of 3.2 mm/yr. RMS scatter is 3.0 mm/yr.

5.4 Comparison Between GIA Model Uplift Predictions and GPS Observations

5.4.1 χ^2 Goodness-of-Fit Test

A χ^2 test is a statistical method of measuring how accurately a given set of observations matches a theoretical or modelled prediction. The difference between the observed quantity and the theoretical quantity at each point is calculated and divided by the uncertainty of the observation. The sum of the square of this quantity for every location in the model is calculated and divided by the number of locations, thus giving a measure of how well the predictions match the data.

(5-2) $$\chi^2 = \frac{1}{n}\sum_n \left(\frac{v_{observed} - v_{calculated}}{\sigma} \right)^2$$

A smaller χ^2 value indicates better agreement between the predictions and observations while larger values indicate that the model is not a good fit to the data.

Calculating the χ^2 of the null hypothesis, or null model, can be very helpful in determining how strong the fits are between the model predictions and the GPS observations. The null hypothesis corresponds to the model featuring no vertical crustal motion. If a model has a larger χ^2 value than the null hypothesis then it means that a null model predicts the observations better.

5.4.2 Degree One Component of GIA Model

Glacial isostatic adjustment in one part of the world is not isolated from what happens elsewhere. Gravitational changes caused by ice mass variations and changes in ocean volume worldwide have an effect on the GIA results seen in Antarctica and thus need to be included in the modelling when comparing to GPS uplift rates. To account for this the Earth models used ran from spherical harmonic degree 2 to 240 where the model

was truncated and an estimate of the global GIA effect was used to account for the first degree. Wu et al. (2010) found a -0.72 mm/yr (uncertainty of 0.06 mm/yr) contribution from global GIA to the geocentre velocity in the z-direction and thus, this value was added to the model results to simulate the degree-one response.

5.4.3 Results

Figures 5.3 and 5.4 show contoured χ^2 values for the asthenosphere, transition zone and lower mantle. The values range between 16 and 2500 showing that none of the uplift predictions fit with the data as well as would be expected. The lowest χ^2 results are seen for an asthenosphere viscosity of 10^{21} Pa·s, a transition zone viscosity of 10^{23} Pa·s and lower mantle viscosity of 2×10^{23} Pa·s. Performing the χ^2 comparison using the null hypothesis (predictions state that no vertical crustal motion will occur) a χ^2 of 42 is found, larger than the minimum value of 16.

5.4.3.1 Averaging Uplift Rates for Stations with Similar Locations

At some sites, two or more nearby (within 3 km) measurements were reported with substantially different uplift rates. The differences are unlikely to be caused by GIA and would be impossible for a postglacial rebound model to replicate. For these stations the average uplift rate was computed and the weighted standard deviation of the observations was assigned to the uncertainty (provided the standard deviation was larger than the original, published uncertainties) (Table 5.3).

Table 5.3: Uplift Rates Averaged by Location[9]

Station	Latitude (degrees)	Longitude (degrees)	Uplift Rate (mm/yr)	Uncertainty in Uplift Rate (mm/yr)
DAV	-68.58	77.97	-1.2	0.7
DUM1	-66.67	140.00	-1.5	0.2
MAW1	-67.60	62.87	-0.8	0.2
SYOG	-69.01	39.58	0.6	0.2
VESL	-71.67	-2.84	1.3	0.3
CAS1	-66.28	110.52	0.5	0.2
OHIG	-63.32	-57.90	7.0	1.0
PALM	-64.78	-64.05	4.8	0.3
SPPT	-64.29	-61.05	7.5	1.8
MCM4 and SCTB	-77.84	166.67	-0.5	1.0
W01	-87.42	-149.43	-3.8	0.8
W02	-85.61	-68.56	-1.4	1.5
W03	-81.58	-28.40	-1.5	1.4
W04	-82.86	-53.20	2.8	1.8
W05	-80.04	-80.56	4.0	1.0
W06	-79.63	-91.28	-4.1	2.3
W07	-80.32	-81.43	5.6	1.5
W08	-75.28	-72.18	4.5	1.5
W09	-82.68	-104.40	6.3	1.3
W12	-78.03	-155.02	6.1	1.0
HAAG	-77.04	-78.29	7.8	0.5

[9] Averaged uplift rates from the GPS observations published in Bevis et al. (2009). The uncertainties are the standard deviation between the uplift rates for a given station unless the standard deviation is less than the published uncertainty for the station.

Figures 5.5 and 5.6 show the χ^2 values throughout the mantle for the averaged data. In this case, χ^2 values ranged between 10 and 4000. Comparison to earlier calculations without the averaging showed that the general pattern of the χ^2 values remained the same for the averaged data as did the resulting best fit viscosity profile. Figure 5.10A and Figure 5.11 compare the observed and predicted uplifts at the West Antarctic stations.

5.4.3.2 Antarctic Peninsula

The highest χ^2 values occur in the Antarctic Peninsula region of the continent. Possible tectonic activity has been suggested (eg. Klepeis and Lawver, 1996 and González-Casado et al., 2000) which could affect uplift in the area. The calculations were repeated without influence from the stations located in the Antarctic Peninsula. As with the averaging, χ^2 values are decreased when the peninsula data are removed from the table of observations but their pattern remains the same (Figures 5.7 and 5.8). With the Antarctic Peninsula stations removed the χ^2 results range from 6 to 550.

5.4.3.3 Systematic Addition to Uplift Rates

In order to determine how robust the minimum χ^2 determination is, the χ^2 analysis was performed for a systematic addition of uplift rates between 2 mm/yr and -2 mm/yr to the original Bevis et al. (2009) observations. There is a broad minimum of χ^2 values indicating that the effect of an additive constant is relatively small (Figure 5.9).

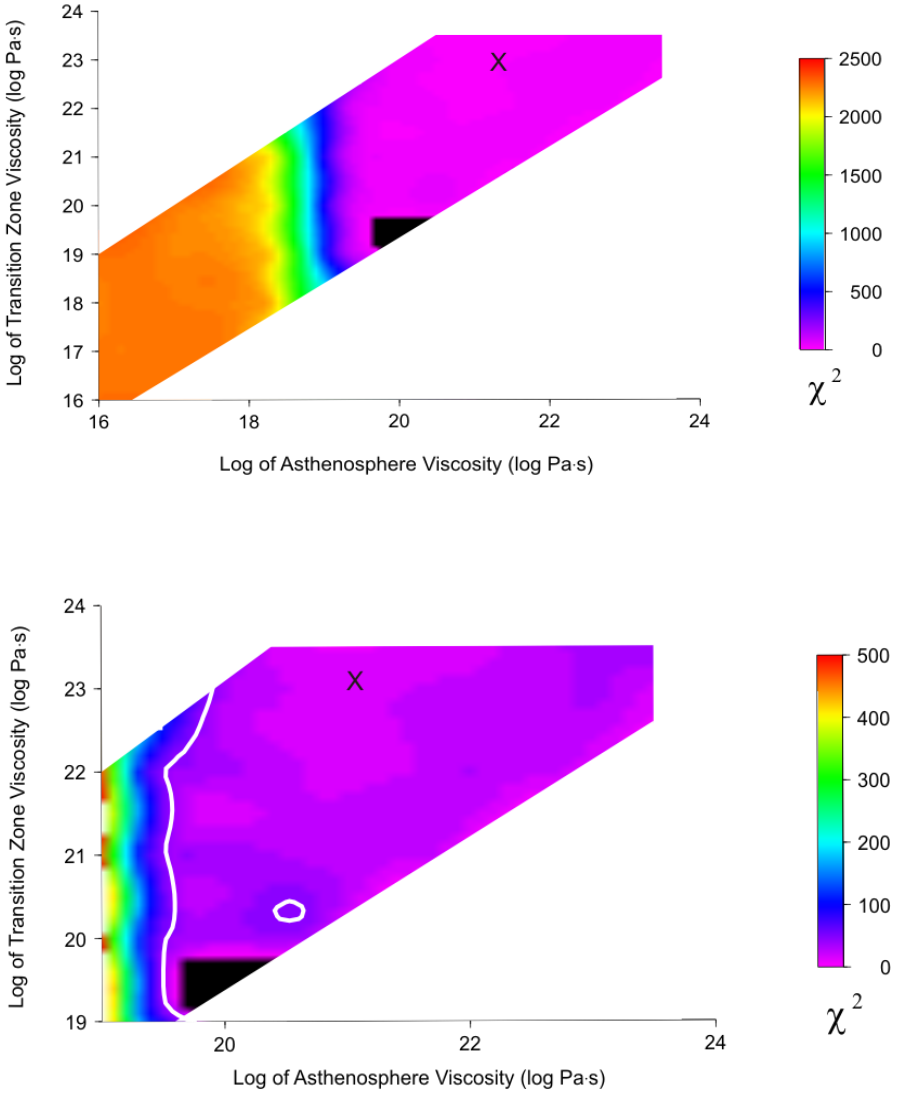

Figure 5.3: (top) χ^2 values for IJ05 predictions and published GPS vertical rates, showing the dependence on asthenosphere and transition zone viscosities. (bottom) Zoomed in version of the top panel for the region with minimum χ^2 values. The X represents the point with the minimum χ^2. The white line shows a contour of the null hypothesis.

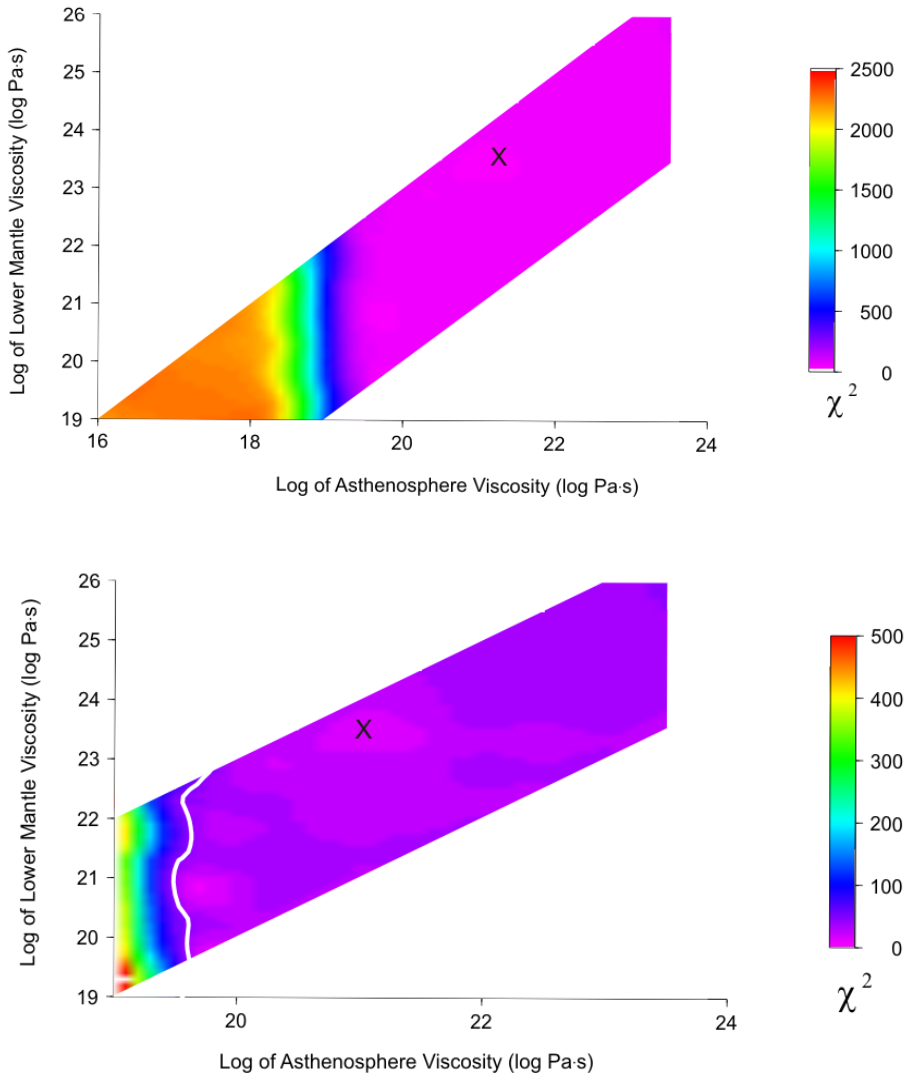

Figure 5.4: (top) χ^2 values for IJ05 predictions and published GPS vertical rates, showing the dependence on asthenosphere and lower mantle viscosities. (bottom) a zoomed in version of the top panel for the region with minimum χ^2 values. The X represents the point with the minimum χ^2. The white line shows a contour of the null hypothesis.

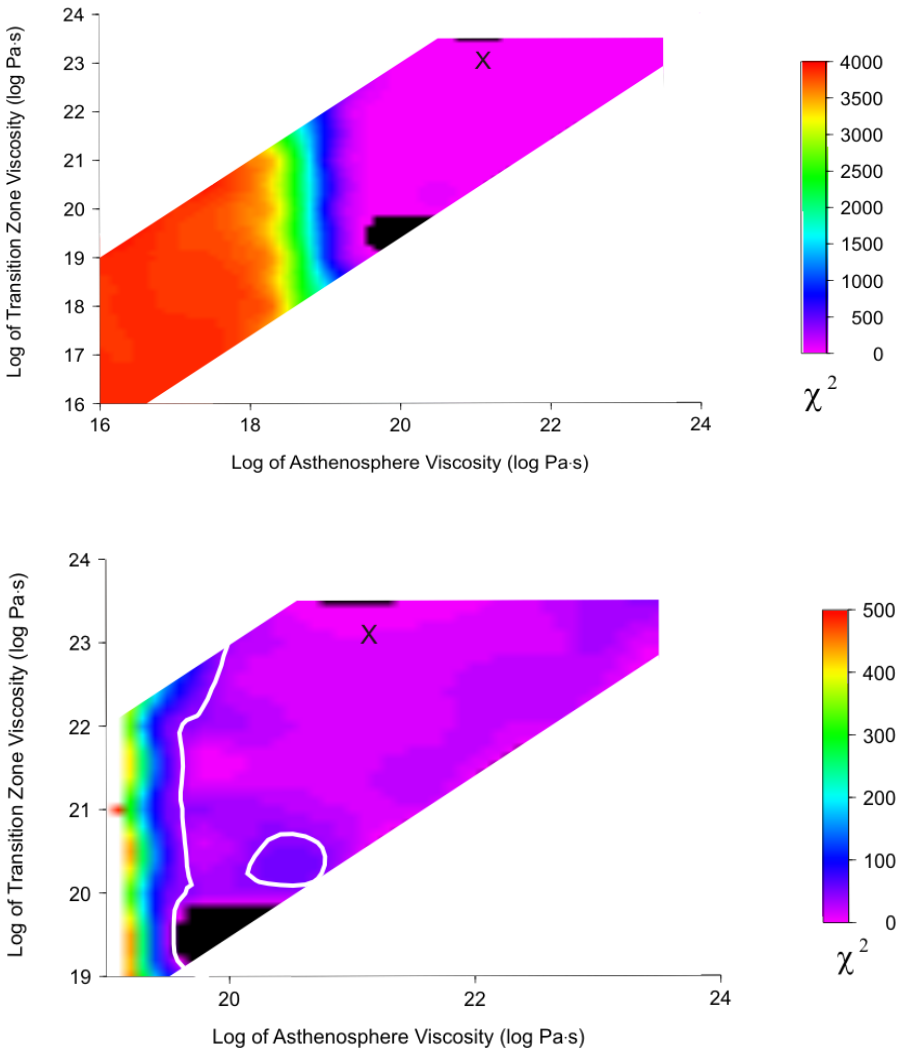

Figure 5.5: (top) χ^2 values for IJ05 predictions and averaged GPS vertical rates, showing the dependence on asthenosphere and transition zone viscosities. (bottom) a zoomed in version of the top panel for the region with minimum χ^2 values. The X represents the point with the minimum χ^2. The white line shows a contour of the null hypothesis.

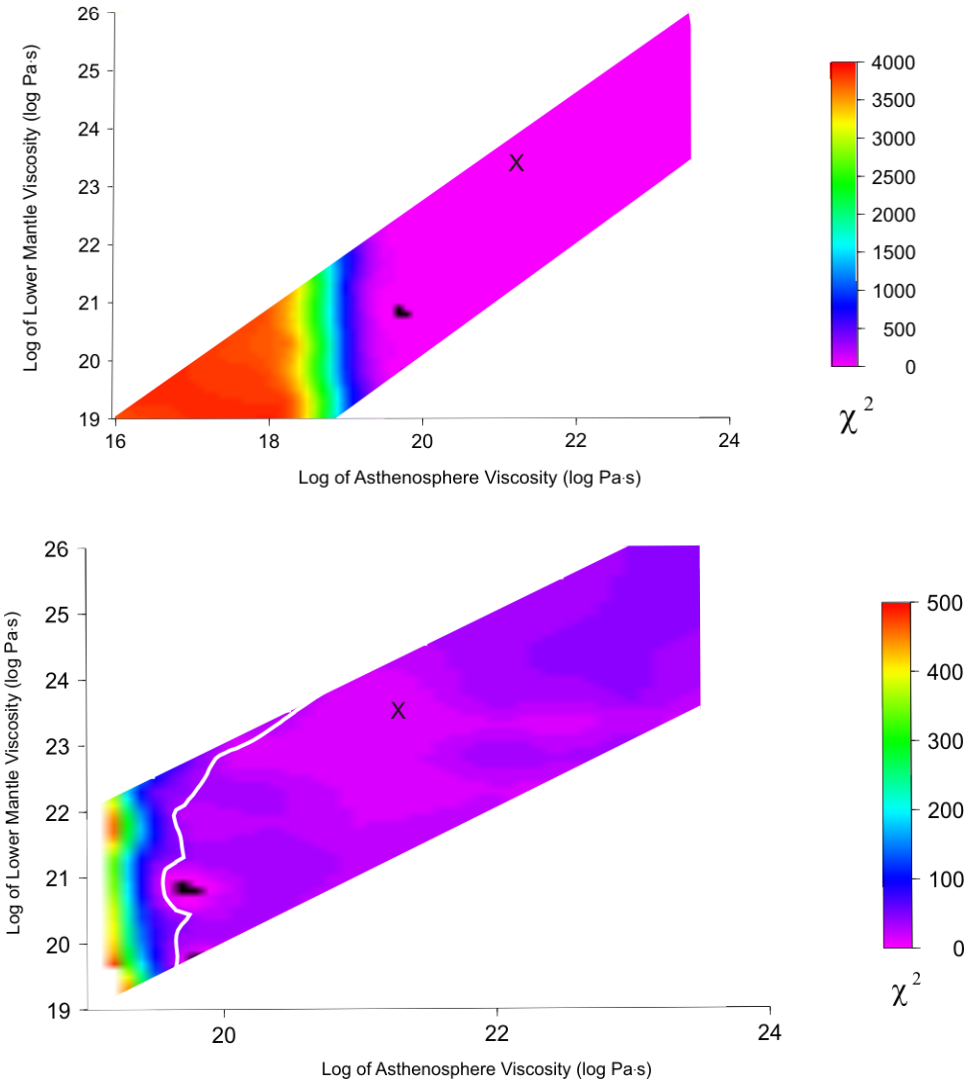

Figure 5.6: (top) χ^2 values for IJ05 predictions and averaged GPS vertical rates, showing the dependence on asthenosphere and lower mantle viscosities. (bottom) a zoomed in version of the top panel for the region with minimum χ^2 values. The X represents the point with the minimum χ^2. The white line shows a contour of the null hypothesis.

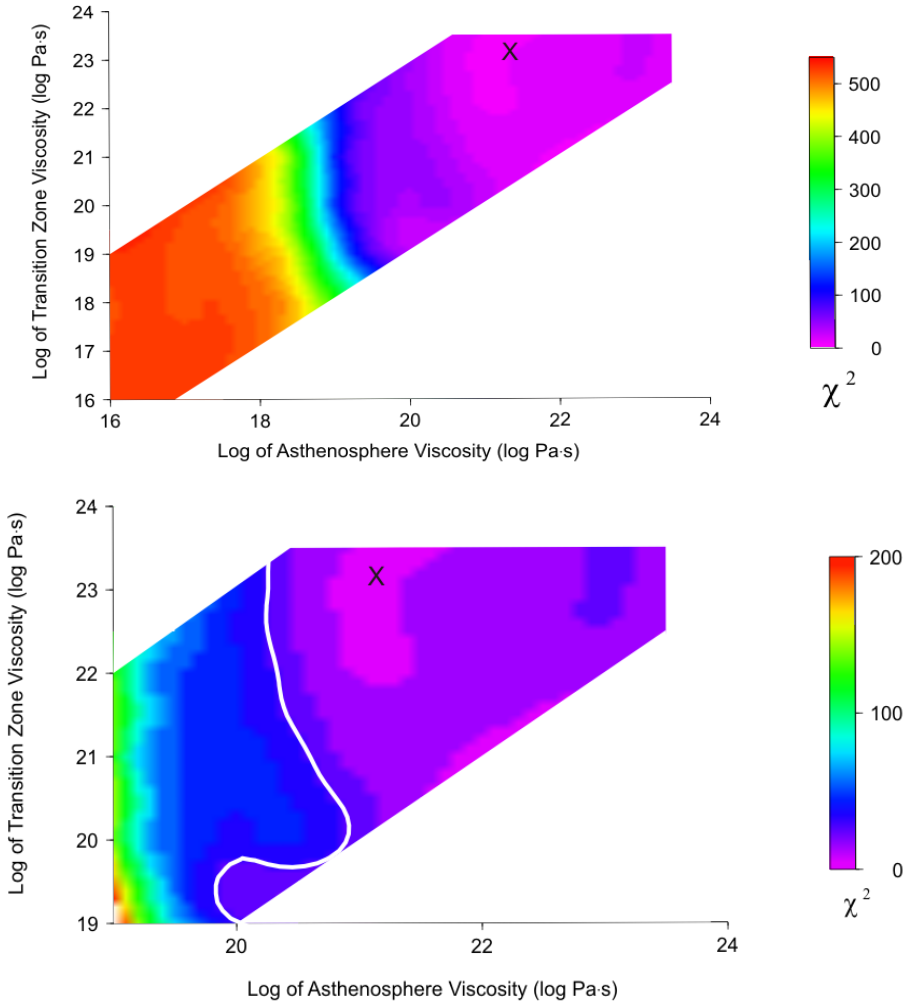

Figure 5.7: (top) χ^2 values for IJ05 predictions and averaged GPS vertical rates with the Antarctic Peninsula stations removed, showing the dependence on asthenosphere and transition zone viscosities. (bottom) a zoomed in version of the top panel for the region with minimum χ^2 values. The X represents the point with the minimum χ^2. The white line shows a contour of the null hypothesis.

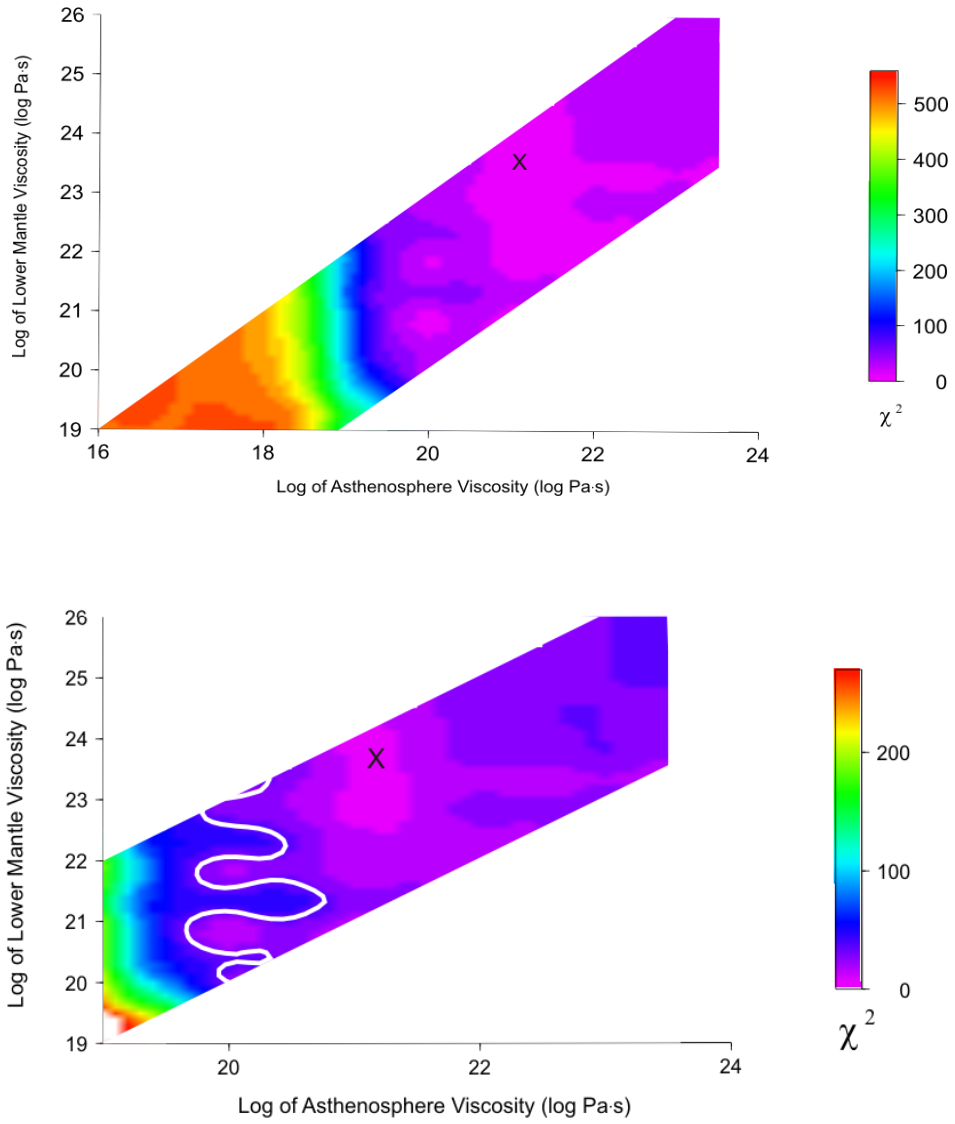

Figure 5.8: (top) χ^2 values for IJ05 predictions and averaged GPS vertical rates with the Antarctic Peninsula stations removed, showing the dependence on asthenosphere and lower mantle viscosities. (bottom) a zoomed in version of the top panel for the region with minimum χ^2 values. The X represents the point with the minimum χ^2. The white line shows a contour of the null hypothesis.

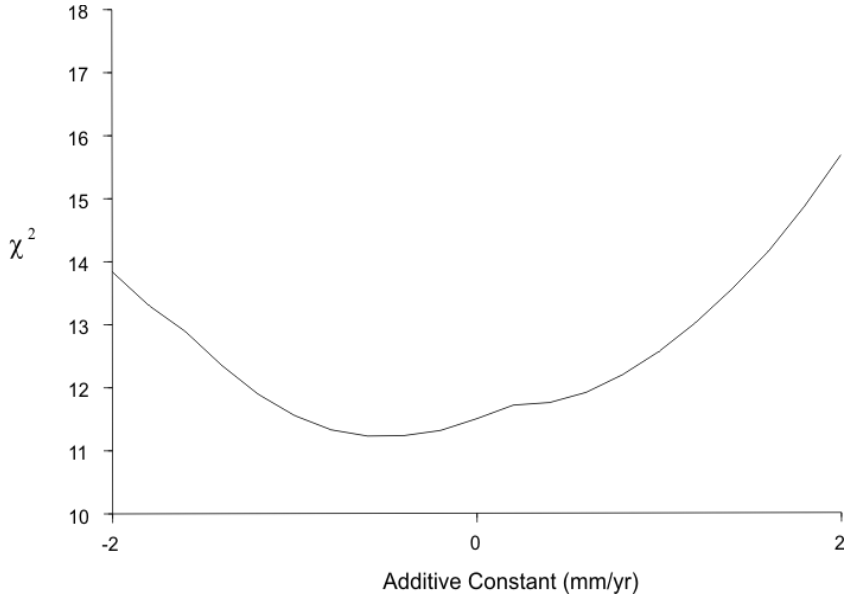

Figure 5.9: χ^2 analysis for a systematic addition of +2 mm/yr to -2 mm/yr to the original GPS observations where the zero offset is the uplift rates published by Bevis et al. (2009).

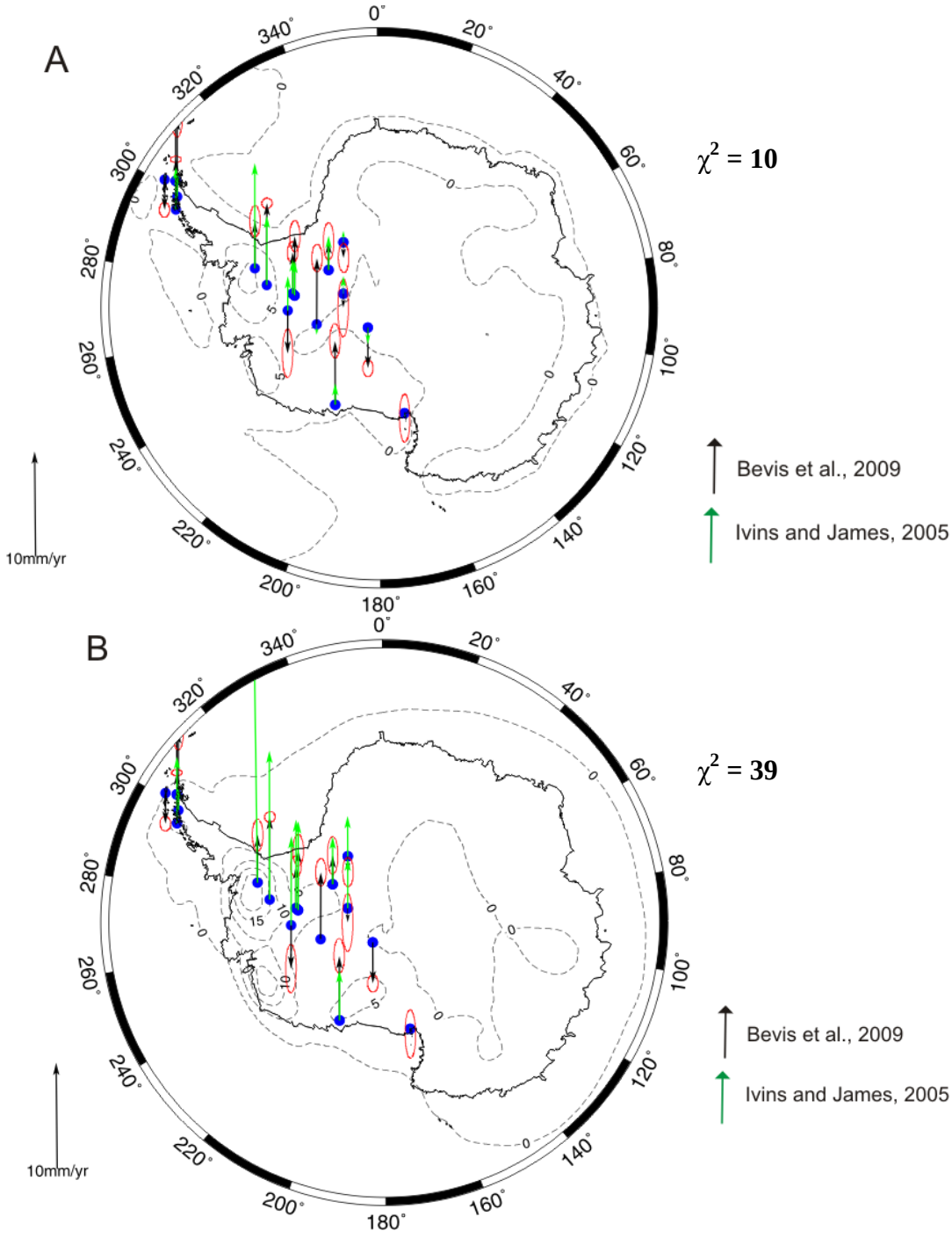

Figure 5.10: Vertical crustal motion rates for West Antarctica. (A) shows the modelled uplift rates for the best fit viscosity profile. (B) shows the uplift rates for the expected viscosity based on the seismic tomography results obtained in Chapter 3. The black arrows represent the averaged GPS observations (with the vertical span of the red ellipses indicating their uncertainties) and the green arrows represent the predicted rates. Dashed contour lines represent IJ05 uplift rates.

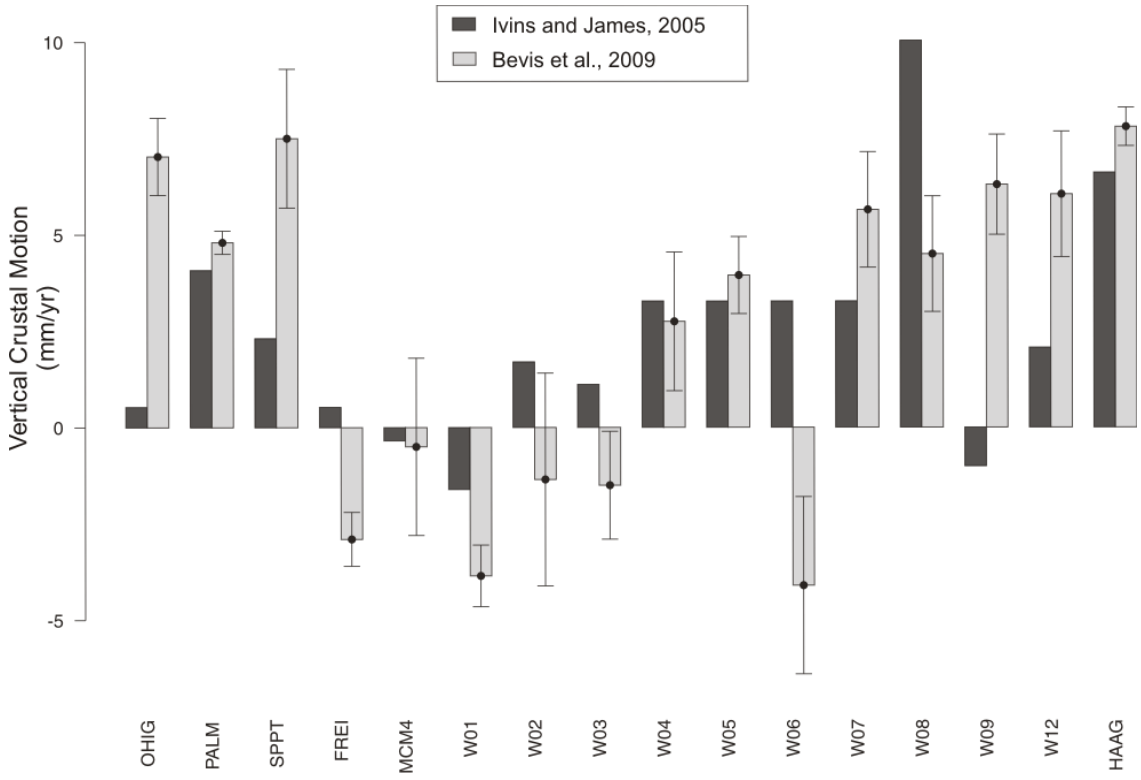

Figure 5.11: Vertical crustal motion for West Antarctica by station for the best fit viscosity profile. Light grey bars represent GPS observations (Bevis et al., 2009) and their associated uncertainties. Dark grey bars represent IJ05 (Ivins and James, 2005) predictions.

5.4.4 Viscosity Expectations versus Best Fit Results

Expectations of West Antarctic mantle viscosity based on the seismic tomography analysis in Chapter 3 and comparisons to the Basin and Range in North America are much lower than the viscosity values found to best fit the GPS data. The expected asthenosphere viscosity is at least two orders of magnitude smaller than the value found to best fit the GPS observed uplift rates. If the GPS observations are correct and they cannot be properly fit by changes to the viscosity profile, then revisions to the ice history

of the model must be made. Figure 5.10B shows the predicted uplift rates for the model predicted by the seismic tomography analysis in Chapter 3 which had an asthenosphere viscosity of 5×10^{19} Pa·s, a transition zone viscosity of 10^{21} Pa·s and a lower mantle viscosity of 2×10^{22} Pa·s. Of the 375 viscosity profiles, 46% lie below the null hypothesis χ^2 value of 42.

5.5 Changes to the Ice Sheet History

If no reasonable viscosity model can explain the observed GPS data then changes to the ice history must be required. Rates of ice melting are assumed to have been constant for the past several hundred years as data that would constrain recent ice thicknesses are more difficult to obtain. At the time that the IJ05 ice model was constructed, the best observational constraints on the present day surface mass balance were 22 km^3/yr in East Antarctica and -48 km^3/yr in West Antarctica (Rignot and Thomas, 2002). These rates were extrapolated backwards in time 150 years to allow paleo data of ancient ice sheet thicknesses to be connected with the present.

5.5.1 Spatial and Temporal Variations in Ice Thickness as Obtained Through Simulated Annealing

To find possible areas where the ice history could be modified to better fit the vertical crustal motion results, the Antarctic ice history used by Ivins and James (2005) was split into 5 geographic regions (Antarctic Peninsula, Ellsworth Land, Transantarctic mountains, central West Antarctica and East Antarctica) and 3 temporal ones (21 kyr BP – 10 kyr BP, 10 kyr BP – 5 kyr BP and 5 kyr BP to present). A multiplier (a value that would be allowed to vary throughout the procedure and was multiplied by the original ice thickness at a given location to create a new ice history) was allotted to each region (15 in total) and, using the method of simulated annealing (Kirkpatrick et al., 1983), the

multiplier was allowed to vary until the predicted vertical crustal uplift rates were comparable to the GPS observations. Each region contained approximately four GPS stations.

The original ice history was used as a starting point for the simulated annealing program (all multipliers began with a value of 1). A random number between 0 and 1 was chosen for each multiplier and was added to or subtracted (the decision made by drawing another random number) from the previous value of the multiplier creating a new set. These new multipliers were then applied to the original ice history and the corresponding uplift rate predictions were calculated using IJ05. As before, a χ^2 calculation was made to evaluate how well the predictions correspond with the observations. A χ^2 value was determined for each geographic region of Antarctica to evaluate which areas experienced a better fit. If the χ^2 misfit was found to be lower than the original value, the changes to the three multipliers in that region were retained. If the misfit was higher than the previous value a random number was drawn and compared to the expression below.

$$P = \exp\left(\frac{\Delta E}{T}\right) \tag{5-3}$$

where ΔE is the difference between the current misfit and the previous one and T is a "temperature" which is slowly decreased. If the random number was less than P the multipliers were retained otherwise the multipliers returned to their previous values. The process is then repeated until the misfit is sufficiently small. The method of allowing some changes to the multipliers that do not decrease misfit allows the function of the ice history to move out of local minima in favour of finding the global minimum. Decreasing the temperature allows fewer misfit-raising multipliers to be accepted

eventually zeroing in on the minimum. The multipliers were allowed to vary between 0.1 and 5. This process was performed for several different mantle viscosity profiles with asthenosphere viscosity ranging from 10^{17} Pa·s to 10^{22} Pa·s, transition zone viscosity ranging from 10^{17} Pa·s to 10^{22} Pa·s, and lower mantle viscosity ranging from 10^{20} Pa·s to 10^{25} Pa·s to determine which profile yielded the minimum χ^2.

The results varied significantly between the geographic regions of Antarctica (Table 5.4). In the Antarctic Peninsula the best fit viscosity profile had an asthenosphere viscosity of 10^{20} Pa·s, a transition zone viscosity of 10^{21} Pa·s and a lower mantle viscosity of 2×10^{22} Pa·s. In the Antarctic Peninsula the multipliers were near 4.0 for the time periods between 21 kyr ago and 5 kyr ago which indicates that a significant increase in past ice thicknesses between Last Glacial Maximum and 5kyr ago was required. Between 5 kyr ago and the present the multiplier indicated a decrease in ice thickness would improve fit.

In Ellsworth Land, the best fit viscosity profile had a constant viscosity of 10^{20} Pa·s. Multipliers again suggest an increase in ice thickness between 21 kyr ago and 5 kyr ago but a decrease between 5 kyr ago and the present.

In the Transantarctic Mountains the best fit viscosity profile was lower (an asthenosphere viscosity of 10^{18} Pa·s, a transition zone viscosity of 10^{18} Pa·s and a lower mantle viscosity of 2×10^{21} Pa·s) and a small increase in the multipliers was observed.

The rest of West Antarctica fit best with a viscosity profile with a constant viscosity through the asthenosphere and transition zone of of 10^{20} Pa·s and a lower mantle viscosity of 10^{22} Pa·s. A moderate increase was seen in the ice thicknesses between 21 kyr ago and 10 kyr ago but a decrease was suggested between 10 kyr ago and

the present. The best fit multipliers, best fit viscosities and minimum χ^2 values are shown in Table 5.4.

For some areas on Antarctica, particularly the Antarctic Peninsula, the past ice thickness multipliers become quite high. It is not expected that the past ice thicknesses would differ from the values obtained through dating methods so significantly. The χ^2 misfit is still very large (14), so the multiplier values are very poorly constrained. Likely, differences in uplift rates seen between the IJ05 predictions and the GPS observations are caused by another source such as tectonics.

Average χ^2 values were found to vary by an additive value of 2 or less from the originally obtained results when selected viscosity profiles were rerun through the simulated annealing program. It was observed that the smallest χ^2 value was significantly less than 2 while the largest value for the AP was not significantly different from the χ^2

Table 5.4: Simulated Annealing Results[10]

Region	Asthenosphere Viscosity	Transition Zone Viscosity	Lower Mantle Viscosity	Multipliers			Null χ^2	χ^2
				21 kyr - 10 kyr	10 kyr - 5 kyr	5 kyr –0 kyr		
AP	10^{20}	10^{21}	2×10^{22}	3.98	3.82	0.81	107.6	14.0
EL	10^{20}	10^{20}	10^{20}	3.99	2.90	0.13	126.2	0.7
TAM	10^{18}	10^{18}	2×10^{21}	2.64	1.84	1.69	6.2	0.6
WA	10^{20}	10^{20}	10^{22}	2.74	0.29	0.39	16.0	4.8

[10] Regions are the Antarctic Peninsula (AP), Ellsworth Land (EL), the Trans Antarctic Mountains (TAM) and central West Antarctica (WA).

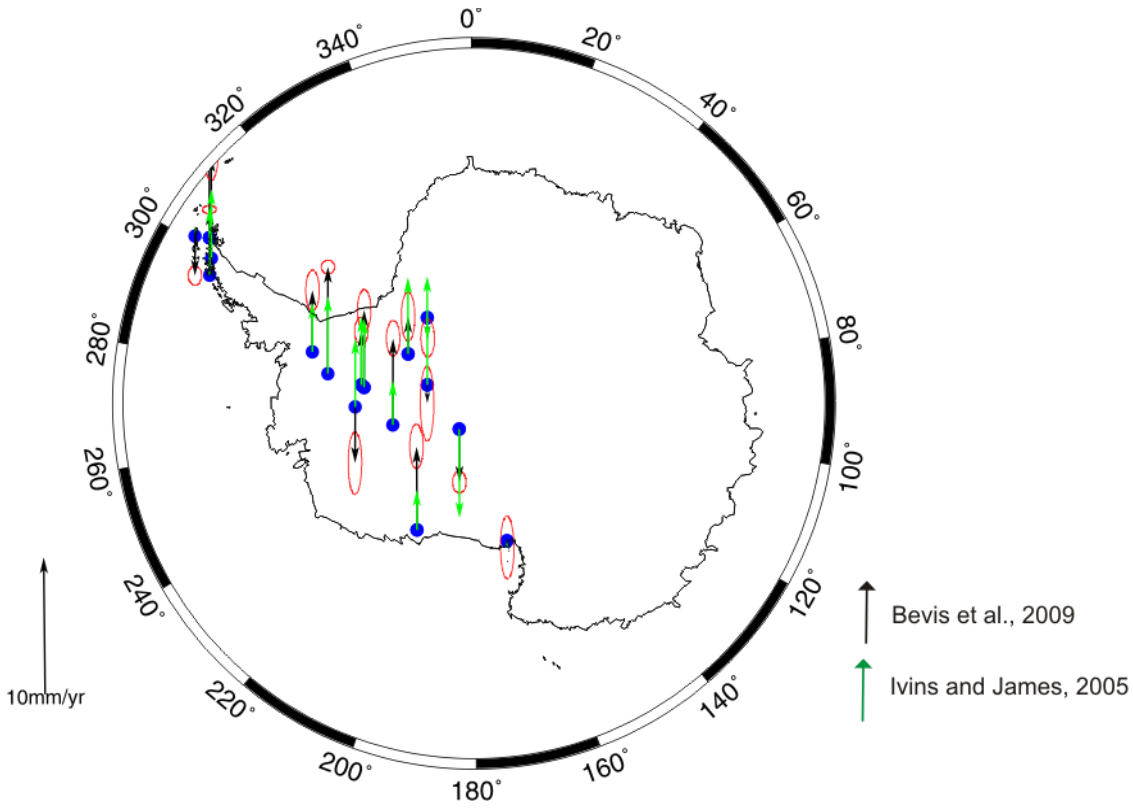

Figure 5.12: Vertical crustal motion rates for West Antarctica. Uplift rates are shown for the best fit viscosity profiles and best fit past ice thickness multipliers obtained through simulated annealing. The black arrows represent the averaged GPS observations (with the red circles indicating their uncertainties) and the green arrows represent the predicted rates.

value for the null hypothesis. A thorough evaluation of the variation of the χ^2 values obtained in the simulated annealing was not performed but could be pursued in future work.

The χ^2 result for the best fit simulated annealing results was 5.5. Figure 5.12 shows the uplift rates for West Antarctica and Figure 5.13 shows the ice thicknesses before and after the simulated annealing procedure.

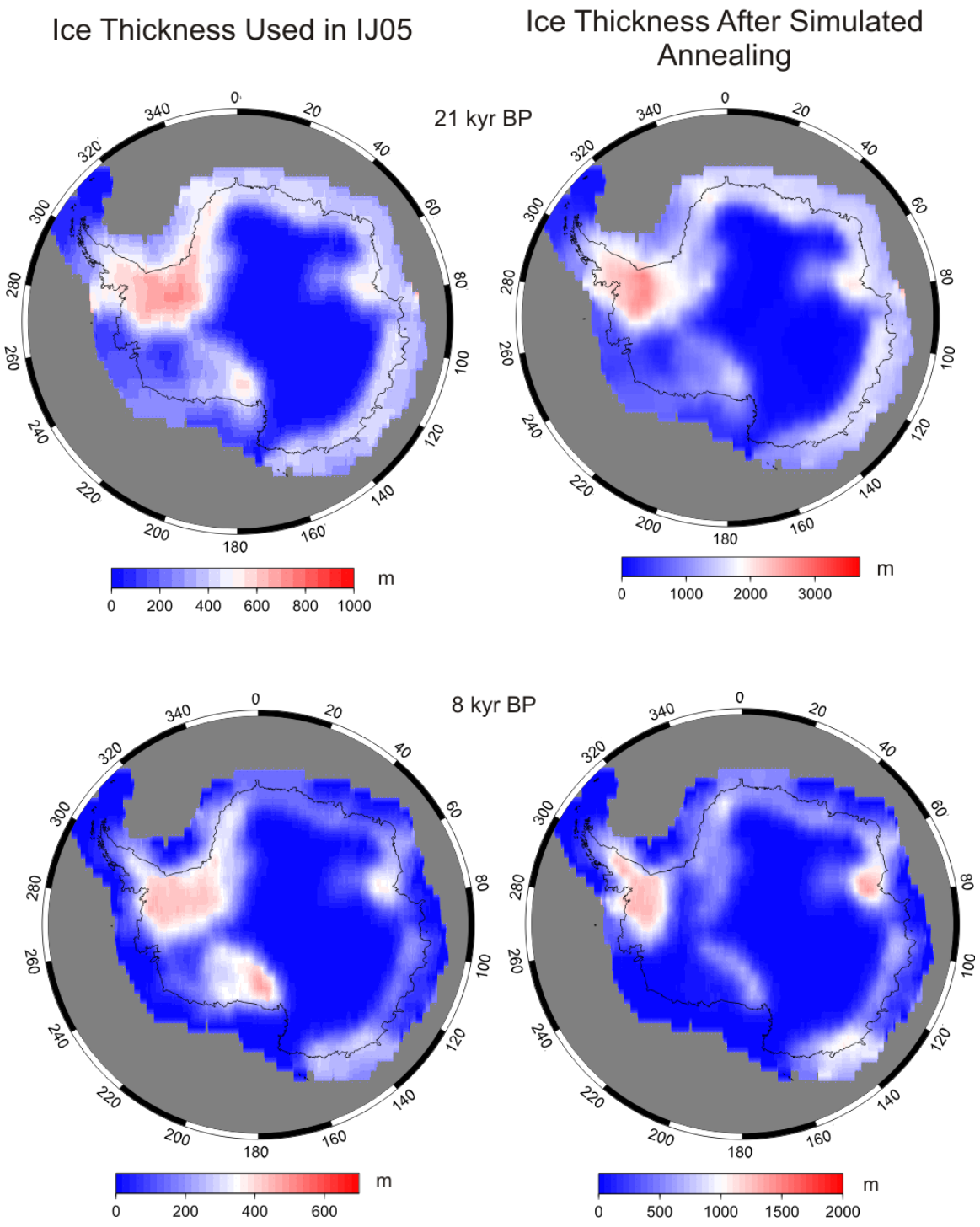
Ice Thickness Used in IJ05
Ice Thickness After Simulated Annealing
21 kyr BP
8 kyr BP
0 200 400 600 800 1000
m
0 1000 2000 3000
m
0 200 400 600
m
0 500 1000 1500 2000
m

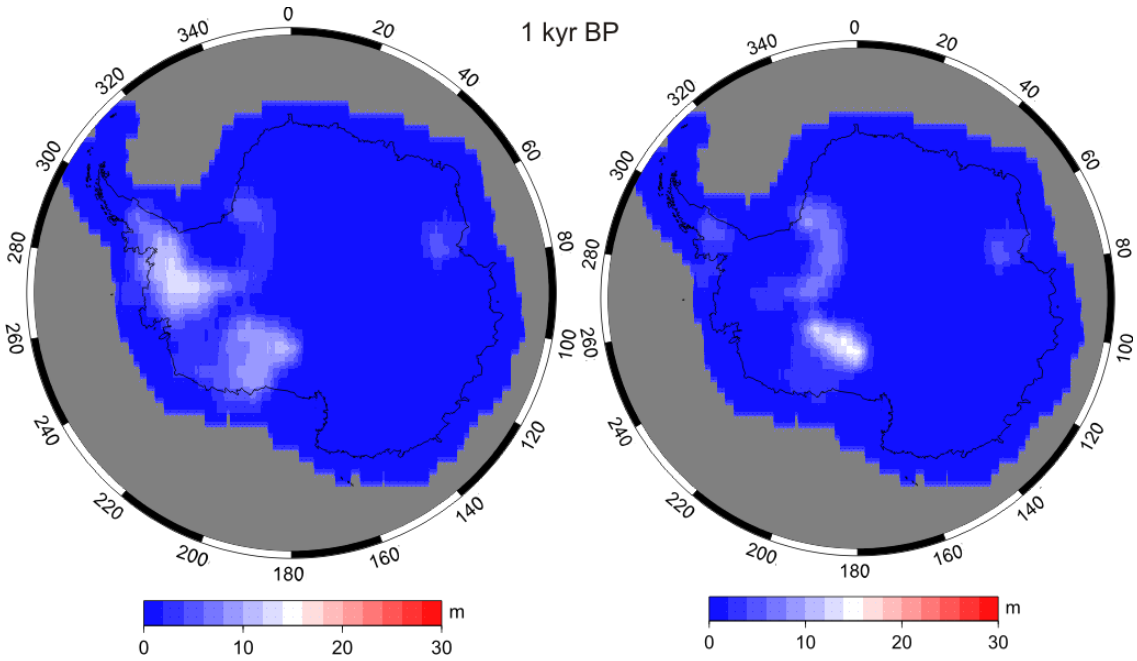

Figure 5.13: Ice thicknesses used by IJ05 (left) and ice thickness obtained through simulated annealing (right) for 21 kyr BP (top), 8kyr BP (middle) and 1 kyr BP (bottom).

5.5.2 Changes to Recent Ice History

Data are largely unavailable to help constrain the most recent ice sheet history in Antarctica. To fill in the model, present day surface mass balance rates are extrapolated back 150 yr while Holocene rates are extrapolated forwards from 800 yr before present.

Table 5.5: Simulated Annealing Focusing on Recent Ice Thickness Changes

Region	Asthenosphere Viscosity	Transition Zone Viscosity	Lower Mantle Viscosity	Multipliers		χ^2
				800 yr BP	150 yr BP	
AP	10^{20}	10^{20}	2×10^{22}	3.34	2.06	19.1
EL	10^{20}	10^{20}	10^{20}	2.73	0.34	1.3
TAM	10^{18}	10^{19}	2×10^{20}	4.70	0.64	1.8
WA	10^{21}	10^{21}	2×10^{22}	3.05	0.21	6.4

To determine whether these assumptions are correct, χ^2 analyses and simulated annealing were performed for ice histories in which only the ice thickness at 150 yr and at 800 yr were allowed to vary.

The best fit viscosity profiles were similar for each region and there was little change in the χ^2 values produced (Table 5.5). The χ^2 for all the regions together was 7.8. As changes in only the most recent ice thicknesses can result in nearly the same level of improvement as changes applied to the entire ice history of Antarctica; these results indicate that revision of the most recent ice thicknesses could have a large effect on the vertical crustal motion results.

5.6 Summary

Predicted vertical crustal motions generated by glacial isostatic adjustment modelling do not agree well with recent Antarctic GPS observations. The Earth models tested here that fit the data best in West Antarctica had high viscosities compared to what is expected in the region (based on the results of Chapters 3 and 4), implying that revision is needed elsewhere in the modelling process.

Past ice thicknesses also have a strong effect on how the crust rebounds and an exploratory investigation was carried out using the simulated annealing technique to see if changes to this aspect would yield better results. Simulated annealing performed on the past ice thicknesses used in IJ05 indicates that the mantle viscosity profile varies between regions of the continent but, in general, a slight increase in ice thicknesses in these regions between Last Glacial Maximum and 5 kyr ago and a slight decrease between 5 kyr ago and the present improves the fit. Ice thicknesses were allowed to increase by up to 5 times the original ice thickness for a given location and time period

but multipliers in the range of 2 or higher are likely too large to be physically plausible. It is not believed that the glaciological and glacial geological constraints are that poor.

Even with changes to the past ice thicknesses there are some areas where the GPS observations do not compare well to the GIA predictions. In the Antarctic Peninsula the stations are located quite close to one another but experience very different vertical crustal motions. Glacial isostatic adjustment causes large scale changes but it cannot be the cause of observations like these. It is possible vertical crustal motion in the Antarctic Peninsula is being caused by other processes such as tectonic activity, or, possibly, very short-wavelength changes in ice mass balance that generate a substantial elastic response.

Chapter 6 – Conclusions

6.1 Seismic Wave Analysis

Changes in seismic wave velocity in the Earth are caused by temperature and compositional variations throughout the planet's interior. By making the assumption that all variations in wave velocity are due to changes in temperature, the viscosity of the mantle can be calculated. Using the Kaufmann et al. (2005) method and seismic wave tomography from S20A (Ekstrom and Dziewonski, 1998), West Antarctic mantle viscosities were found to be approximately 5×10^{19} Pa·s in the asthenosphere, 10^{21} Pa·s in the transition zone and 2×10^{22} Pa·s in the lower mantle. These results agree with predictions for the region based on comparisons to analogous locations in more thoroughly studied areas of the world.

6.2 Elevation, Crustal Thickness and Mantle Viscosity

An analysis by Hyndman (2010) in the North American Cordillera indicates a first order correlation between elevation, crustal thickness and the viscosity of the mantle. High elevations paired with thinner than expected crust indicate that the mantle is hot and, thus, has a low viscosity, while thicker crust indicates that the mantle is cold with a higher viscosity. Applying this analysis to Antarctica, it can be seen that regions expected to be cratonic in nature, like East Antarctica, fall nearer to the cold mantle trend while areas expected to have thinner crust, like West Antarctica, fall nearer to the hot mantle linear regression.

6.3 Comparing GPS-Observed Uplift Rates and GIA Model Predictions

Recent GPS observations of Antarctic vertical crustal motion (Bevis et al., 2009) were compared to uplift rates calculated through glacial isostatic adjustment modelling

(Ivins and James, 2005). Using a χ^2 measure of goodness-of-fit, predicted uplift rates which best matched the GPS observations were found by sampling a wide range of mantle viscosity profiles and comparing the predicted vertical crustal motion rates to the GPS observations.

The viscosity profile that best fit the observations consisted of an asthenosphere viscosity of 10^{21} Pa·s, a transition zone viscosity of 10^{23} Pa·s and a lower mantle viscosity of 2×10^{23} Pa·s. These values are much higher than expected for the mantle viscosity underlying West Antarctica, indicating that changes to the ice history are needed. Simulated annealing performed on the past ice thicknesses showed that changes to recent ice history provided a better fit in some regions.

Certain regions, like the Antarctic Peninsula, could not be fit well by any model. This could be a result of factors influencing uplift rates besides glacial isostatic adjustment, such as tectonic processes or the elastic response of the Earth to near-by ice mass changes.

6.4 Summary and Recommendations for Future Research

Seismic wave tomography and elevation and crustal thickness comparisons in Antarctica both demonstrate a low viscosity mantle in West Antarctica and a high viscosity mantle in East Antarctica, as is expected from the geological setting. Comparisons between GPS observations and GIA model predictions of vertical crustal motion demonstrate that much higher than expected mantle viscosities are required in West Antarctica for the predictions and observations to agree. This does not agree with the seismic tomography and elevation/crustal thickness analyses, indicating that changes to the ice load history are needed. Preliminary investigation using simulated annealing

reveals that changes to the recent ice thickness history has significant effects on the vertical crustal motion caused by glacial isostatic adjustment. Further work could generate a new ice-sheet history that is consistent with the geological and glaciological record and that generates vertical motion predictions for a plausible mantle viscosity profile that are in agreement with GPS observations.

The limited density, both in space and duration, of available data has proven to be a limiting factor in this study. Additional seismic wave studies specific to Antarctica would be of great use in determining the mantle viscosity beneath the continent. More crustal thickness studies throughout Antarctica would help to constrain the results used when comparing elevation and crustal thickness, possibly allowing hot and cold mantle trends for the continent to be calculated. Longer time series of GPS observations, obtained from denser networks in West Antarctica, would help discriminate between GIA-induced vertical crustal motion and the motion caused by other factors. Constraints on the most recent ice thicknesses (during the last millenium) could greatly improve modelling of the response of the Earth to past and recent ice mass changes. A promising avenue for further exploration would be to apply the simulated annealing technique over smaller regions to see if a better agreement with GPS observations could be reached while appropriately constraining recent ice mass changes.

Bibliography

Ackert Jr., R. P., Barclay, D. J., Borns Jr., H. W., Calkin, P. E., Kurz, M. D., Fastook, J. L., Steig, E. J., 1999. Measurements of past ice sheet elevations in interior West Antarctica. Science. 286, 276-280.

Altamimi, Z., Angermann, D., Argus, D., Blewitt, G., Boucher, C., Chao, B., Drewes, H., Eanes, R., Feissel, M., Ferland, R., Herring, T., Holt, B., Johannson, J., Larson, K., Ma, C., Manning, J., Meertens, C., Nothnagel, A., Pavlis, E., Petit, G., Ray, J., Ries, J., Schemeck, H., Sillard, P., Watkins, M., 2001. The Terrestrial Reference Frame and the Dynamic Earth. EOS, Transactions, American Geophysical Union. 82, 273.

Altamimi, Z., Boucher, C., Gambis, D., 2005. Long-term stability of the terrestrial reference frame. Advances in Space Research. 36, 342-349.

Altamimi, Z. and Collilieux, X., 2009. IGS contribution to the ITRF. Journal of Geodesy. 83, 375-383.

Anderson, J. B., Shipp, S. S., Lowe, A. L., Wellner, J. S., Mosola, A. B., 2002. The Antarctic Ice Sheet during the Last Glacial Maximum and its subsequent retreat history: A review. Quaternary Science Reviews. 21, 49-70.

Bassin, C., Laske, G., Masters, G., 2000. The Current Limits of Resolution for Surface Wave Tomography in North America. EOS Trans AGU. 81, F897.

Bayer, B., Geissler, W. H., Eckstaller, A., Jokat, W., 2009. Seismic imaging of the crust beneath Dronning Maud Land, East Antarctica. Geophysical Journal International. 178, 860-876.

Behrendt, J. C., Saltus, R., Damaske, D., McCafferty, A., Finn, C. A., Blankenship, D., Bell, R. E., 1996. Patterns of late Cenozoic volcanic and tectonic activity in the West Antarctic rift system revealed by aeromagnetic surveys. Tectonics. 15, 660-676.

Bennett, R. A., Wernicke, B. P., Niemi, N. A., Friedrich, A. M., Davis, J. L., 2003. Contemporary strain rates in the northern Basin and Range province from GPS data. Tectonics. 22, 3-1 - 3-31.

Bentley, M., 2009. The Antarctic palaeo record and its role in improving predictions of future Antarctic Ice Sheet change. J.Quat.Sci.

Bentley, M. J. and Anderson, J. B., 1998. Glacial and marine geological evidence for the ice sheet configuration in the Weddell Sea-Antarctic Peninsula region during the Last Glacial Maximum. Antarctic Science. 10, 309-325.

Bevis, M., Kendrick, E., Smalley Jr., R., Dalziel, I., Caccamise, D., Sasgen, I., Helsen, M., Taylor, F. W., Zhou, H., Brown, A., Raleigh, D., Willis, M., Wilson, T., Konfal, S., 2009. Geodetic measurements of vertical crustal velocity in West Antarctica and the implications for ice mass balance. Geochemistry, Geophysics, Geosystems. 10, .

Bills, B. G., Adams, K. D., Wesnousky, S. G., 2007. Viscosity structure of the crust and upper mantle in western Nevada from isostatic rebound patterns of the late Pleistocene Lake Lahontan high shoreline. Journal of Geophysical Research B: Solid Earth. 112, .

Bills, B. G., Currey, D. R., Marshall, G. A., 1994. Viscosity estimates for the crust and upper mantle from patterns of lacustrine shoreline deformation in the eastern Great Basin. Journal of Geophysical Research. 99, 22,059-22,086.

Bromley, G. R. M., Hall, B. L., Stone, J. O., Conway, H., Todd, C. E., 2010. Late Cenozoic deposits at Reedy Glacier, Transantarctic Mountains: implications for former thickness of the West Antarctic Ice Sheet. Quaternary Science Reviews. 29, 384-398.

Chopelas, A. and Boehler, R., 1992. Thermal expansivity in the lower mantle. Geophysical Research Letters. 19, 1983-1986.

Cooper, A. K., Davey, F. J., Behrendt, J. C., 1987. Seismic stratigraphy and structure of the Victoria Land Basin, Western Ross Sea, Antarctica. The Antarctic Continental Margin: Geology and Geophysics of the Western Ross Sea. 5 B, 27-76.

Cooper, A. K., Trey, H., Pellis, G., Cochrane, G., Egloff, F., Busetti, M., 1997. Crustal Structure of the Southern central trough, western Ross Sea. The Antarctic Region: Geological Evolution and Processes. 637-642.

Dalziel, I. W. D. and Elliot, D. H., 1982. West Antarctica: problem child of Gondwanaland. Tectonics. 1, 3-19.

Denton, G. H. and Hughes, T. J., 2000. Reconstruction of the Ross ice drainage system, Antarctica, at the last glacial maximum. Geografiska Annaler, Series A: Physical Geography. 82, 143-166.

Dietrich, R., Rülke, A., Ihde, J., Lindner, K., Miller, H., Niemeier, W., Schenke, H. -., Seeber, G., 2004. Plate kinematics and deformation status of the Antarctic Peninsula based on GPS. Global and Planetary Change. 42, 313-321.

Dziewonski, A. M. and Anderson, D. L., 1981. Preliminary reference Earth model. Physics of the Earth and Planetary Interiors. 25, 297-356.

Ekström, G. and Dziewonski, A. M., 1998. The unique anisotropy of the Pacific upper mantle. Nature. 394, 168-172.

Farrell, W. E., 1972. Deformation of the Earth by surface loads. Rev.Geophys.Space Phys. 10, 761-797.

Fernandes, R. M. S., Ambrosius, B. A. C., Noomen, R., Bastos, L., Combrinck, L., Miranda, J. M., Spakman, W., 2004. Angular velocities of Nubia and Somalia from continuous GPS data: Implications on present-day relative kinematics. Earth and Planetary Science Letters. 222, 197-208.

Fogwill, C. J., Bentley, M. J., Sugden, D. E., Kerr, A. R., Kubik, P. W., 2004. Cosmogenic nuclides ^{10}Be and ^{26}Al imply limited Antarctic Ice Sheet thickening and low erosion in the Shackleton Range for >1 m.y. Geology. 32, 265-268.

Forsyth, D. W., 1985. Subsurface loading and estimates of the flexural rigidity of continental lithosphere. Journal of Geophysical Research. 90, 12,623-12,632.

Forte, A. M. and Mitrovica, J. X., 2001. Deep-mantle high-viscosity flow and thermochemical structure inferred from seismic and geodynamic data. Nature. 410, 1049-1056.

González-Casado, J. M., Giner-Robles, J. L., López-Martínez, J., 2000. Bransfield Basin, Antarctic Peninsula: Not a normal backarc basin. Geology. 28, 1043-1046.

Gore, D. B., Rhodes, E. J., Augustinus, P. C., Leishman, M. R., Colhoun, E. A., Rees-Jones, J., 2001. Bunger Hills, East Antarctica: Ice free at the Last Glacial Maximum. Geology. 29, 1103-1106.

Hall, B. L., 2009. Holocene glacial history of Antarctica and the sub-Antarctic islands. Quaternary Science Reviews. 28, 2213-2230.

Hall, B. L., Baroni, C., Denton, G. H., 2004. Holocene relative sea-level history of the Southern Victoria Land Coast, Antarctica. Global and Planetary Change. 42, 241-263.

Hall, B. L., Denton, G. H., Overturf, B., 2001. Glacial Lake Wright, a high-level antarctic lake during the LGM and early holocene. Antarctic Science. 13, 53-60.

Hasterok, D. and Chapman, D. S., 2007. Continental thermal isostasy: 1. Methods and sensitivity. Journal of Geophysical Research B: Solid Earth. 112, .

Huerta, A. D. and Harry, D. L., 2007. The transition from diffuse to focused extension: Modeled evolution of the West Antarctic Rift system. Earth and Planetary Science Letters. 133.

Hyndman, R. D., 2010. The consequences of Canadian Cordillera thermal regime in recent tectonics and elevation: a review. Canadian Journal of Earth Science. 47, 621-632.

Hyndman, R. D. and Currie, C. A., 2011. Why is the North America Cordillera high? Hot backarcs, thermal isostasy, and mountain belts. Geology. 39, 783-786.

Hyndman, R. D., Currie, C. A., Mazzotti, S., Fredericksen, A., 2009. Temperature control of continental lithosphere elastic thickness, Te vs Vs. Earth and Planetary Science Letters. 277, 539-548.

Isanina, E. V., Krupnova, N. A., Popov, S. V., Masolov, V. N., Lukin, V. V., 2009. Deep structure of the Vostok Basin, East Antarctica as deduced from seismological observations. Geotectonics. 43, 221-225.

Ivins, E. R. and James, T. S., 2005. Antarctic glacial isostatic adjustment: A new assessment. Antarctic Science. 17, 541-553.

Ivins, E. R. and Sammis, C. G., 1995. On lateral viscosity contrast in the mantle and the rheology of low- frequency geodynamics. Geophysical Journal International. 123, 305-322.

James, T. S. and Ivins, E. R., 1998. Predictions of Antarctic crustal motions driven by present-day ice sheet evolution and by isostatic memory of the Last Glacial Maximum. Journal of Geophysical Research B: Solid Earth. 103, 4993-5017.

Jin, Y. K., Lee, J., Hong, J. K., Nam, S. H., 2009. Is subduction ongoing in the South Shetland Trench, Antarctic Peninsula?: New constraints from crustal structures of outer trench wall. Geosciences Journal. 13, 59-67.

Johnson, J. S., Bentley, M. J., Gohl, K., 2008. First exposure ages from the Amundsen Sea Embayment, West Antarctica: The Late quaternary context for recent thinning of Pine Island, Smith, and Pope Glaciers. Geology. 36, 223-226.

Karato, S., 1993. Importance of anelasticity in the interpretation of seismic tomography. Geophysical Research Letters. 20, 1623-1626.

Kaufmann, G., Wu, P., Ivins, E. R., 2005. Lateral viscosity variations beneath Antarctica and their implications on regional rebound motions and seismotectonics. Journal of Geodynamics. 39, 165-181.

Kearey, P., Klepeis, K.A., Vine, F.J., 2009. Global Tectonics. Third Edition.

Kearey, P. and Vine, F. J., 1996. Global tectonics. Second edition. Global Tectonics. Second Edition.

Kirkpatrick, S., Gelatt Jr., C. D., Vecchi, M. P., 1983. Optimization by simulated annealing. Science. 220, 671-680.

Klepeis, K. A. and Lawver, L. A., 1996. Tectonics of the Antarctic-Scotia plate boundary near Elephant and Clarence Islands, West Antarctica. Journal of Geophysical Research B: Solid Earth. 101, 20211-20231.

Klosko, E. R., Russo, R. M., Okal, E. A., Richardson, W. P., 2001. Evidence for a rheologically strong chemical mantle root beneath the Ontong-Java Plateau. Earth and Planetary Science Letters. 186, 347-361.

Leitch, A. M. and Yuen, D. A., 1989. Internal heating and thermal constraints on the mantle. Geophysical Research Letters. 16, 1407-1410.

Leitchenkov, G., Guseva, J., Gandyukhin, V., Grikurov, G., Kristoffersen, Y., Sand, M., Golynsky, A., Aleshkova, N., 2008. Crustal structure and tectonic provinces of the Riiser-Larsen Sea area (East Antarctica): Results of geophysical studies. Marine Geophysical Researches. 29, 135-158.

Lemke, P., Ren, J., Alley, R.B., Allison, I., Carrasco, J., Flato, G., Fuji, Y., Kaser, G., Mote, P., Thomas, R.H., Zhang, T., 2007. Observations: Changes in Smow, Ice and Frozen Ground. in: Anonymous Climate Change 2007: The Physical Science Basis. Contribution of Working Group 1 to the Fourth Assessment Report of the Intergovernmental Panel on Climate Change. Cambridge University Press, Cambridge, United Kingdom and New York, NY, USA, .

Lewis, B. T. R. and Dorman, L. M., 1970. Experimental isostasy, 2, An isostatic model for the United States derived from gravity and topographic data. J.Geophys.Res. 75, 3367-3386.

Licht, K. J., 2004. The Ross Sea's contribution to eustatic sea level during meltwater pulse 1A. Sedimentary Geology. 165, 343-353.

Liu, K., Levander, A., Niu, F., Miller, M. S., 2011. Imaging crustal and upper mantle structure beneath the Colorado Plateau using finite frequency Rayleigh wave tomography. Geochemistry, Geophysics, Geosystems. 12, .

Lythe, M. B. and Vaughan, D. G., 2001. BEDMAP: A new ice thickness and subglacial topographic model of Antarctica. Journal of Geophysical Research B: Solid Earth. 106, 11335-11351.

Mackintosh, A., White, D., Fink, D., Gore, D. B., Pickard, J., Fanning, P. C., 2007. Exposure ages from mountain dipsticsk in Mac. Robertson Land, East Antarctica, indicate little change in ice-sheet thickness since the Last Glacial Maximum. Geology. 35, 551-554.

Maldonado, A., Larter, R. D., Aldaya, F., 1994. Forearc tectonic evolution of the South Shetland Margin, Antarctic Peninsula. Tectonics. 13, 1345-1370.

Mooney, W. D., Laske, G., Masters, T. G., 1998. CRUST 5.1: A global crustal model at 5° × 5°. Journal of Geophysical Research B: Solid Earth. 103, 727-747.

Peltier, W. R., 1985. The LAGEOS constraint on deep mantle viscosity: results from a new normal mode method for the inversion of viscoelastic relaxation spectra. Journal of Geophysical Research. 90, 9411-9421.

Ranalli, G., 1995. Rheology of the Earth, 2nd ed. Chapman and Hall, .

Rignot, E., Bamber, J. L., Van Den Broeke, M. R., Davis, C., Li, Y., Van De Berg, W. J., Van Meijgaard, E., 2008. Recent Antarctic ice mass loss from radar interferometry and regional climate modelling. Nature Geoscience. 1, 106-110.

Rignot, E. and Thomas, R. H., 2002. Mass balance of polar ice sheets. Science. 297, 1502-1506.

Ritzwoller, M. H., Shapiro, N. M., Barmin, M. P., Levshin, A. L., 2002. Global surface wave diffraction tomography. Journal of Geophysical Research B: Solid Earth. 107, ESE 4-1 - 4-13.

Shapiro, N. M. and Ritzwoller, M. H., 2004. Inferring surface heat flux distributions guided by a global seismic model: Particular application to Antarctica. Earth and Planetary Science Letters. 223, 213-224.

Tackley, P. J., 1993. Effects of strongly temperature-dependent viscosity on time-dependent, three-dimensional models of mantle convection. Geophysical Research Letters. 20, 2187-2190.

Toracinta, R. E., Oglesby, R. J., Bromwich, D. H., 2004. Atmospheric response to modified CLIMAP ocean boundary conditions during the last glacial maximum. Journal of Climate. 17, 504-522.

Turcotte, D.L., Schubert, G., 2002. Geodynamics, Second Edition ed. Cambridge, .

van Wijk, J. W., Lawrence, J. F., Driscoll, N. W., 2008. Formation of the Transantarctic Mountains related to extension of the West Antarctic Rift system. Tectonophysics. 117.

Velicogna, I., 2009. Increasing rates of ice mass loss from the Greenland and Antarctic ice sheets revealed by GRACE. Geophysical Research Letters. 36, .

Verleyen, E., Hodgson, D. A., Milne, G. A., Sabbe, K., Vyverman, W., 2005. Relative sea-level history from the Lambert Glacier region, East Antarctica, and its relation to deglaciation and Holocene glacier readvance. Quaternary Research. 63, 45-52.

Verleyen, E., Hodgson, D. A., Sabbe, K., Vyverman, W., 2004. Late quaternary deglaciation and climate history of the Larsemann Hills (East Antarctica). Journal of Quaternary Science. 19, 361-375.

Waddington, E. D., Conway, H., Steig, E. J., Alley, R. B., Brook, E. J., Taylor, K. C., White, J. W. C., 2005. Decoding the dipstick: Thickness of Siple Dome, West Antarctica, at the Last Glacial Maximum. Geology. 33, 281-284.

Wahr, J., Wingham, D., Bentley, C., 2000. A method of combining ICESat and GRACE satellite data to constrain Antarctic mass balance. Journal of Geophysical Research B: Solid Earth. 105, 16279-16294.

Wallner, H. and Schmeling, H., 2010. Rift induced delamination of mantle lithosphere and crustal uplift: A new mechanism for explaining Rwenzori Mountains' extreme elevation? International Journal of Earth Sciences. 99, 1511-1524.

Watanabe, O., Jouzel, J., Johnsen, S., Parrenin, F., Shoji, H., Yoshida, N., 2003. Homogeneous climate variability across East Antarctica over the past three glacial cycles. Nature. 422, 509-512.

Watts, A. B. and Burov, E. B., 2003. Lithospheric strength and its relationship to the elastic and seismogenic layer thickness. Earth and Planetary Science Letters. 213, 113-131.

Wernicke, B., 1992. Cenozoic extensional tectonics of the U.S. Cordillera. The Cordilleran Orogen. 3 G, 553-581.

Winberry, J. P. and Anandakrishnan, S., 2004. Crustal structure of the West Antarctic rift system and Marie Byrd Land hotspot. Geology. 32, 977-980.

Wingham, D. J., Shepherd, A., Muir, A., Marshall, G. J., 2006. Mass balance of the Antarctic ice sheet. Philosophical Transactions of the Royal Society A: Mathematical, Physical and Engineering Sciences. 364, 1627-1635.

Wu, P. and Johnston, P., 1998. Validity of using flat-earth finite element models in the study of postglacial rebound. Dynamics of the Ice Age Earth: A Modern Perspective. 191-202.

Wu, X., Heflin, M. B., Schotman, H., Vermeersen, B. L. A., Dong, D., Gross, R. S., Ivins, E. R., Moore, A. W., Owen, S. E., 2010. Simultaneous estimation of global present-day water transport and glacial isostatic adjustment. Nature Geoscience. 3, 642-646.

Zandt, G., Myers, S. C., Wallace, T. C., 1995. Crust and mantle structure across the Basin and Range-Colorado Plateau boundary at 37°N latitude and implications for Cenozoic extensional mechanism. Journal of Geophysical Research. 100, 10,529-10,548.

Zeyen, H., Volker, F., Wehrle, V., Fuchs, K., Sobolev, S. V., Altherr, R., 1997. Styles of continental rifting: Crust-mantle detachment and mantle plumes. Tectonophysics. 278, 329-352.

Zwartz, D., Bird, M., Stone, J., Lambeck, K., 1998. Holocene sea-level change and ice-sheet history in the Vestfold Hills, East Antarctica. Earth and Planetary Science Letters. 155, 131-145.